Joint Learning of Discriminative Low-dimensional Image Representations Based on Dictionary Learning and Two-layer Orthogonal Projections

Xian Wei, *Member, IEEE,* Hao Shen, *Member, IEEE,* Yuanxiang Li, *Member, IEEE,* Xuan Tang, *Member, IEEE,* Bo Jin, *Member, IEEE,* Lijun Zhao, *Member, IEEE,* and Yi Lu Murphey, *Fellow, IEEE*

***Abstract*—This work investigates the problem of efficiently learning discriminative low-dimensional representations of multi-class large-scale image objects. We propose a generic deep learning approach by taking advantages of Convolutional Neural Networks (CNN), sparse dictionary learning, and orthogonal projections. CNN is not only powerful on feature extraction, but also robust to spatial variance and changes. Sparse dictionary learning is well known for disentangling nonlinear underlying discriminative factors in data. The orthogonal projection is a notable efficient tool to project multi-class data onto low dimensional discriminative subspace. The proposed procedure can be summarized as follows. At first, a CNN is employed to extract high-dimensional (HD) preliminary convolutional features. Secondly, to avoid the high computational cost of direct sparse coding on HD CNN features, we present to learn sparse representation (SR) in an orthogonal projected space over a task-driven sparsifying dictionary. We then exploit the discriminative projection on SR. The whole learning process is treated as a joint optimization problem of trace quotient maximization, which involves the CNN parameters, the orthogonal projection on CNN features, the dictionary and the discriminative projection on sparse codes. The related cost function is well defined on product manifold of the Stiefel manifold, the Oblique manifold, and the Grassmann manifold. It is optimized via a geometrical stochastic gradient descent algorithm. Finally, the quality of dictionary and projections learned by the proposed approach is further investigated in terms of image classification. The experimental results show that the approach can achieve a strongly competitive performance with state-of-the-art image classification methods.**

***Index Terms*—Representation learning, sparse representation, trace quotient, dimension reduction, dictionary learning, orthogonal projection, geometrical stochastic gradient algorithm, supervised discrimination learning.**

I. Introduction

Learning appropriate low-dimensional (LD) representations of data plays a critical role as a preprocessing procedure for the success of discrimination learning algorithms, because of its convenience on geometric interpretations and its parsimony on computations [1], [2]. One core discovery in LD discriminative representation learning is that deep architecture of representations, i.e., multiple levels of representation, enables prominent disentanglibility of underlying factors that explains discrepancy underneath the observed signals, e.g., images [3]. Specifically, the performance of deep learning is strongly dependent on the choice and organization of various general purpose priors, such as sparsity [4], depth of explanatory factors [5], and manifold [6]. In this work, we investigate a deep joint learning paradigm for finding approximate LD representations of multi-class large-scale imagery objects, which is capable of carrying the useful information to facilitate the task of discrimination learning, such as object categorization.

A. Related Work

Conventional approaches often represent the multi-class high-dimensional (HD) data collection as the input that is lying in some underlying subspaces [7], [8] or a low-dimensional smooth manifold [6], [9], called dimension reduction (DR). They seek to convey underlying discriminative structure of interest from original HD space to low dimensional ones. The related learning process relies on the decomposition of data relationship matrix over an *undercomplete* bases set, namely, dictionary [10]. Such a setting covers prominent examples like Linear Discriminant Analysis (LDA) [7], Semi-supervised LDA (SDA) [11], Sufficient Dimensionality Reduction (SDR) [12], supervised Non-Negative Matrix Factorization (NMF) [2], Spectral Clustering (SC) [8], etc., which encode the HD data as a *dense undercomplete* representation over a dictionary with orthogonal columns [10], called orthogonal projections. This kind of orthogonal projections are well-known efficient tools to project multi-class data onto low-dimensional subspaces, by virtue of the low computational complexity and the low sample complexity [10]. However, they often suffer from the noise corruption, and the low efficiency for extracting nonlinear discrimination between images [13]–[15] due to their shallow linear projection architecture.

Different from data decomposition over an orthogonal *undercomplete* dictionary like LDA, sparse representation (SR) was originally developed as an instrument to leverage the underlying sparse structure of data over an *overcomplete* dictionary [14], [16]. The method relies on the assumption that a signal $\mathbf{x} \in \mathbb{R}^m$ can be represented as a linear combination

X. Wei and X. Tang are with Fujian Institute of Research on the Structure of Matter, Chinese Academy of Sciences, China. H. Shen is with the Technical University of Munich, Germany and fortiss GmbH, Munich, Germany. B.Jin is with Shanghai Key Lab for Trustworthy Computing, School of Computer Science and Software Engineering, East China Normal University, China. Yuanxiang Li is with School of Aeronautics & Astronautics, Shanghai Jiao Tong University, Shanghai 200240, China. Lijun Zhao is with State Key Laboratory of Robotics and System, Harbin Institute of Technology, Harbin 150006, China. Y. L. Murphey is with Department of Electrical and Computer Engineering, University of Michigan-Dearborn, Dearborn, MI 48128, USA.

This work has been supported by the German Research Foundation (DFG) under Grant No. KL 2189/9-1, the CAS Pioneer Hundred Talents Program (Type C) under Grant No.2017-122, and the National Science Found for Young Scholars under Grant No. 61806186.

of a few atoms in a dictionary $\mathbf{D} \in \mathbb{R}^{m \times q}, m \ll q$. Formally, this can be described as

$$\mathbf{x} = \mathbf{D}\boldsymbol{\alpha} + \boldsymbol{\epsilon}, \tag{1}$$

where $\boldsymbol{\alpha} \in \mathbb{R}^q$ is the sparse coefficient vector, and $\boldsymbol{\epsilon} \in \mathbb{R}^m$ is the residual term. It has achieved great success with wide applications in signal reconstruction, denoising and inpainting [4], [17], [18]. These methods can be considered as *data-driven sparse representation* approaches.

On the other hand, current research focuses on exploiting the discrimination of sparse representation, such as learning or constructing dictionaries for face recognition [19], handwritten digit classification [20], [21], object categorization [22], [23], or human action recognition [23], [24], etc. It has been empirically observed that the structure in sparse domain could make the hidden patterns more prominent and easier to be captured, and sparse coefficients are often interpreted as the extracted features to promote the task of discriminative prediction. For example, the work in [14], [22], [25] incorporates linear classifiers with sparse representation to jointly learn a sparsifying dictionary and a classifier. Similarly, adopting sparse representations in a classical expected risk minimization formulation leads to the so-called *task-driven dictionary learning* approaches, specifically for supervised learning tasks, cf. [20], [26].

One common scheme shared by these methods is to learn multiple dictionaries or class-specific dictionaries for training samples and then to employ a set of binary classifiers in a "one-versus-all" or "one-versus-one" strategy for solving multi-class classification problems, cf. [20], [25], [26]. Such a learning scheme is beneficial to the final predictors, but it is susceptible to suffer from time-consuming and storage burden when encountering a large number of classes. Moreover, in the practical application of visual recognition, there is another serious issue in most SR based algorithms, i.e., finding an appropriate faction of data as shown in Eq. (1) can be prohibitively expensive when the dimensionality of the raw input is huge [10]. These inputs could be the raw images with high resolution, or their preliminary features that are extracted by preprocessing representation learners. Typical preliminary representation learners include deep convolutional neural networks (CNN) [27], [28], and the spatial pyramid pooling (SPP) strategy [29]–[31]. Both of them can generate a fixed-length, but HD representation, regardless of the raw image size/scale and robust to spatial variance, cf. [28], [32]. Learning these extremely redundant dictionaries for high-resolution images or their HD representations is often difficult by using regular computing resources [10]. Although constructing convolutional layers associated with neural network regression, e.g., VGG-16 [27] and Inception series [33], [34], is a popular way to extract label-driven representations, such a strategy often requires very large amount of labeled training samples, resulting in prohibitive training efforts for a large number of classes.

B. Motivation and Main Contributions

With the aim of efficiently learning discrimination between images for multi-class large-scale objects, we propose to construct an efficient algorithm to jointly learn discriminative features on sparse coefficients. Our joint learning scheme can be summarized as the following four steps. At first, a CNN is conducted to extract HD preliminary features. Secondly, in order to reduce the time consumption of learning sparse codes of CNN features, we adopt a popular way to learn sparse representations in a reduced feature subspace of input CNN feature space. Such a reduced subspace is achieved by a traditional orthogonal DR projection. Thirdly, we present to directly learn a linear discriminative orthogonal projection on sparse coefficients. Finally, classical linear classifiers, such as SVM or k-NN, are applied to classify acquired LD features. Thus, the whole learning system (an example is depicted in Fig. 1) is developed which involves the CNN parameters, and a triple of matrix parameters, i.e., the orthogonal projection matrix on original CNN features, the dictionary matrix and the discriminative projection matrix on sparse codes. By treating the CNN features as the input, we construct an appropriate cost function, in which the triple matrix parameters are well defined on a product manifold of the Stiefel manifold, the Oblique manifold and the Grassmann manifold, respectively. We finally employ a gradient descent algorithm on smooth manifold to jointly maximize the cost function. We call this system except the CNN stage as *Jointly Optimized dictionary learning and two-layer Orthogonal Projections for learning discriminative LOW-dimensional Image Representations (JoopLow)* in the rest of this paper.

A preliminary work on modeling low-dimensional representation in sparse domain was briefly presented in [21], which focused on tinny image classification with unsupervised settings. However, the full investigation of the *JoopLow* model has not been systematically conducted. In this work, we fully investigate the potential of the *JoopLow* model for sparse convolutional LD image representation learning, the optimization and its typical application, i.e., categorization. In particular, we first construct a three-layer representation learning block, which benefits from both sparse coding and orthogonal DR projection. We then extend such a *JoopLow* model to the CNN architecture for discrimination learning on large-scale images. Finally, we fully explore the potential of *JoopLow* model in multi-class object categorization, which achieves a competitive performance with state-of-the-art CNN based classification methods.

The main contributions of this work can be summarized in three aspects: i) This paper presents a deep learning approach to learn low dimensional discrminative image representations by taking advantage of CNN, sparse dictionary learning and orthogonal projections. CNN is not only powerful on feature extraction but also robust to spatial variance and changes. Sparse dictionary learning is well known for disentangling nonlinear underlying discriminative factors in data and the orthogonal projection is a prominent efficient tool to project multi-class data onto low-dimensional subspace. The computational efficiency and the discriminative capability are both leveraged. ii) By exploring the differentiability of sparse representations with respect to a given dictionary, this work treats the solution to *JoopLow* as a problem of jointly learning parameters restricted on approximate matrix manifolds.

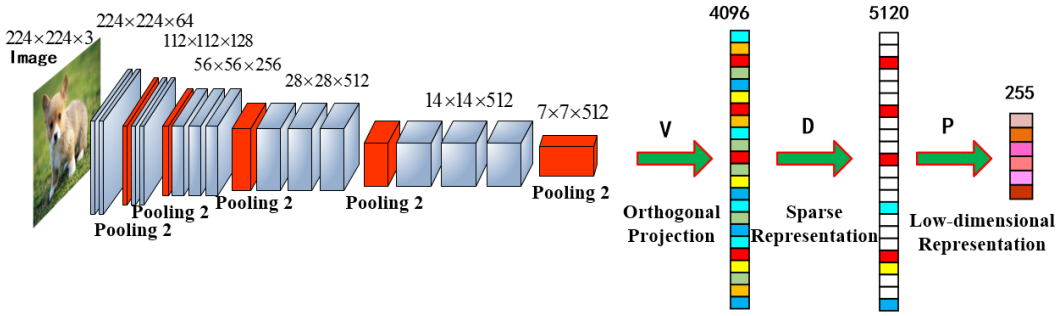

Fig. 1. An example using proposed algorithmic paradigm (VGG-16 *JoopLow*) for classification on Caltech-256 dataset [35]. First, a 224 by 224 crop of an image (with 3 color planes) is presented as the data input. Then, preliminary representations with the size of $7 \times 7 \times 512$ are acquired by applying VGG-16 on the data input with the setting in [27]. Finally, the low-dimensional representations (with the dimension of 255) are learned via training the proposed *VGG-16 JoopLow*. In the figure, $\mathbf{V}, \mathbf{D}, \mathbf{P}$ denotes the orthogonal DR projection, the dictionary and the final discriminative projection, respectively.

Hence, by leveraging both the differentiability of the problem cost function over parameters and the gradient updates in Riemannian manifolds, the commonly used mini-batch based stochastic gradient descent (SGD) algorithm can be employed to optimize the cost function. iii) In this work, we present a Riemannian stochastic gradient descent algorithm, which can reduce the dimension of optimization problems compared with solving the problem in their ambient Euclidean space. iv) The learned orthogonal projections are capable of being adapted to sparse structures of sparse representation over CNN features. Hence, it can get a robust performance when meeting the worse training image pairs, such as the number of training samples is small.

C. Paper Structure and Notations

The rest of this paper is organized as follows. In Section II, we start with a brief introduction of sparse representations and then investigate its sample complexity. In Section III, we construct a generic cost function for learning both a sparsifying dictionary and orthogonal transformations. A geometric stochastic gradient algorithm is developed in Section IV, Section V presents the setting of implementations and several numerical experiments. Finally, we conclude our work in Section VI.

In this work, vectors are denoted by bold lower case letters and matrices by upper case ones. We denote by $\boldsymbol{I}_n$ the $n \times n$-identity matrix, $\mathbf{1}_k$ the k dimensional all-ones column vector, $\mathbf{1}_{k\times k}$ the $k \times k$ all-ones square matrix, $\|\cdot\|_F$ the Frobenius norm of matrices, $\boldsymbol{v}_i$ the i^{th} column of matrix $\boldsymbol{\mathcal{V}}$, $\boldsymbol{E}_{ij}$ a matrix whose i^{th} entry in the j^{th} column is equal to one, and all others are zero, $\mathrm{tr}(\cdot)$ the trace of a matrix, $\boldsymbol{v}_i$ the i^{th} column of matrix $\mathbf{V}$, and, $\mathcal{R}(\cdot)$ the full vector of a sparse representation.

II. Sparse Coding and Sample Complexity

In this section, we first briefly review some state of the art results of sparse coding with Elastic-net prior, which is the core component of the proposed *JoopLow*. Then, the sample complexity is provided to estimate how much the empirical cost function deviates from its expectation to the sparse coding problem. The estimate of sample complexity plays a critical role on improving computational efficiency of the *JoopLow*.

A. Sparse Coding

In order to exploit sparse factorization of Eq. (1), it is crucial to find a dictionary that allows the signal $\mathbf{x}_i$ to be represented accurately with a coefficient vector $\boldsymbol{\alpha}_i$ that is as sparse as possible. Let $\mathbf{X} := [\mathbf{x}_1, \ldots, \mathbf{x}_n] \in \mathbb{R}^{m\times n}$ be the matrix containing the n independent training samples arranged as its columns, the task of dictionary learning focuses on finding the best dictionary to sparsely represent the elements of $\mathbf{X}$. Formally, let $\mathbf{A} := [\boldsymbol{\alpha}_1, \ldots, \boldsymbol{\alpha}_n] \in \mathbb{R}^{q\times n}$ contain the corresponding n sparse transform coefficient vectors, a common approach to the classical dictionary learning techniques [4], [18], is the optimization problem

$$\min_{\mathbf{D}\in\mathcal{S}(m,q),\mathbf{A}\in\mathbb{R}^{q\times n}} \sum_{i=1}^{n} \tfrac{1}{2}\|\mathbf{x}_i - \mathbf{D}\boldsymbol{\alpha}_i\|_2^2 + g(\boldsymbol{\alpha}_i). \tag{2}$$

Therein, the first term penalizes the reconstruction error of sparse representations, the second term $g : \mathbb{R}^q \to \mathbb{R}^+$ is a function that promotes the sparse structure of $\boldsymbol{\alpha}$, and $\mathcal{S}(m, q)$ is some predefined admissible set of solutions in $\mathbb{R}^{m\times q}$ for the dictionary.

Once given an overcomplete dictionary $\mathbf{D} \in \mathcal{S}(m, q)$ $(q > m)$, there are several ways to solve the sparse representation problem in Eq. (1). If sparsity is measured by employing a combination of the ℓ_1- and the ℓ_2-norm, i.e.,

$$g_e(\boldsymbol{\alpha}) := \lambda_1\|\boldsymbol{\alpha}\|_1 + \lambda_2\|\boldsymbol{\alpha}\|_2^2, \tag{3}$$

a solution to the elastic net problem [36], i.e.,

$$\boldsymbol{\alpha}^* := \operatorname*{argmin}_{\boldsymbol{\alpha}\in\mathbb{R}^r} \tfrac{1}{2}\|\mathbf{x} - \mathbf{D}\boldsymbol{\alpha}\|_2^2 + \lambda_1\|\boldsymbol{\alpha}\|_1 + \tfrac{\lambda_2}{2}\|\boldsymbol{\alpha}\|_2^2, \tag{4}$$

yields a convenient way to obtain the sparse representation. The two regularisation parameters $\lambda_1 \in \mathbb{R}^+$ and $\lambda_2 \in \mathbb{R}^+$ are chosen to ensure the stability and the uniqueness of the solution. In this work, we restrict each column $\mathbf{d}_i \in \mathbb{R}^m$ of $\mathbf{D}$ to have unit norm, i.e.,

$$\mathcal{S}(m, q) := \left\{\mathbf{D} \in \mathbb{R}^{m\times q} \middle| \, \mathrm{rk}(\mathbf{D}) = m, \|\mathbf{d}_i\|_2 = 1\right\}, \tag{5}$$

which is a product of $(m-1)$-dimensional unit spheres, and is hence a $q(m-1)$ dimensional smooth manifold, known as Oblique manifold [18], [37]. Such a constraint on the dictionary $\mathbf{D} \in \mathcal{S}(m, q)$ is commonly employed in various dictionary learning procedures to avoid the scale ambiguity problem.

TABLE I
THIS TABLE SHOWS THE DIMENSIONS OF CONMEN CNN AND SPP FEATURES FOR RAW IMAGES. THE CNN FEATURES DENOTE THE 1-DIMENSIONAL COLUMN VECTORS SET AFTER THE FLATTENING LAYER.

Features	Raw image	SPP [31]	AlexNet-5 [38]	OverFeat-7 [39]	ZF-5 [40]	VGG-16 [27]	SPP-net [28]
Dimension m	256×256 $= 65536$	21×1024 $= 21504$	$6 \times 6 \times 256$ $= 9216$	$6 \times 6 \times 1024$ $= 36864$	$6 \times 6 \times 256$ $= 9216$	$7 \times 7 \times 512$ $= 25088$	21×256 $= 5376$

B. Sample Complexity of Dictionary Learning

A fundamental question in dictionary learning process of Eq. (2) is the sample complexity issue, which represents the minimum required number of training-samples to successfully optimize the problem (2). Recalling the sparse representation problem defined in Eq. (4), the quality of how well a signal can be sparsely coded for a dictionary is evaluated via the function

$$f_{\mathbf{x}}(\mathbf{D}) := \inf_{\boldsymbol{\alpha}\in\mathbb{R}^r} \tfrac{1}{2}\|\mathbf{x}-\mathbf{D}\boldsymbol{\alpha}\|_2^2 + g_e(\boldsymbol{\alpha}).$$

Given n independent training samples $\mathbf{X} := [\mathbf{x}_1, \ldots, \mathbf{x}_n] \in \mathbb{R}^{m\times n}$ with an unknown probability $\mathbb{P}$, the average quality of the sparse representation is measured via

$$F_{\mathbf{X}}(\mathbf{D}) := \tfrac{1}{n}\sum_{i=1}^{n} f_{\mathbf{x}_i}(\mathbf{D}). \tag{6}$$

Minimizing Eq. (6) leads to the dictionary learning problem (2). The bound for the generalization error of the empirical minimizer, i.e., the function (6) to its expectation, is computed by

$$\sup_{\mathbf{D}\in\mathcal{S}(m,q)} \left|F_{\mathbf{X}}(\mathbf{D}) - \mathbb{E}_{\mathbf{x}\sim\mathbb{P}} f_{\mathbf{x}}(\mathbf{D})\right| \le \eta(n,m,q,L) \tag{7}$$

with "overwhelming" probability. Therein,

$$\eta(n,m,q,L) := 2\sqrt{\frac{\beta\log n}{n}} + \sqrt{\frac{\beta + t/\sqrt{8}}{n}} \tag{8}$$

with

$$\beta := (mq/8)\max\{\log(6\sqrt{8}L), 1\},$$

in which L and t denote two constants, cf. [10]. Here, n indicates the *sample complexity*, i.e., the number for finding the best dictionary $\mathbf{D} \in \mathcal{S}(m,q)$ to sparsely represent $\mathbf{X}$. When $\eta(n,m,q,L)$ is fixed, it is easy to find that

$$n \propto mq. \tag{9}$$

Furthermore, the covering number bound for the constraint set $\mathcal{S}(m,q)$ is given by

$$\mathcal{N}(\mathcal{S}(m,q),\epsilon) \le (1+2/\epsilon)^{mq} \tag{10}$$

with a constant $\epsilon > 0$.

These theoretical results indicate that the computational complexity of sparse coding depends on the choice of dictionary size, m and q. The computational load will become prohibitively expensive when m and q are large.

III. THE PROPOSED JOINT LEARNING FRAMEWORK

In this section, we construct a three-layer joint representation learning block, which leverages both aforementioned sparse coding and orthogonal DR projections. In order to reduce the sample complexity of sparse coding, we first construct the sparse coding problem in orthogonal projected space. Then, we present the *JoopLow* cost function, which adopts the construction of sparse coding with convex priors in the framework of Trace Quotient maximization to extract LD discriminative representations of sparse representations of input image features. We finally extend the *JoopLow* block to the CNN architecture for discrimination learning on large-scale images.

A. Learning sparse dictionary in orthogonal projected space

For a given data point $\mathbf{x} \in \mathbb{R}^m$, which could be a raw image with high dimension, CNN features [27], [28], or a spatial pyramid pooling vector (SPP) of a picture of an object [29], [31]. The dimensions of them are often high, see Table I. For example, the corresponding sample complexity of sparse coding on VGG-16 features [27] is much larger than 6×10^8, i.e., mq with $q > m$ and $m = 25088$, according to Eq. (7), Eq. (8) and Eq. (9). As discussed in Section II-B, it intuitively suggests that directly learning sparsifying dictionary of CNN and SPP features is often a challenge for common computing resources [10]. Furthermore, the very high dimensionality associated with limited labeled training samples often suffers from the so-called the *small sample size problem* [41]. Therefore, it is necessary to conduct a additional learning paradigm to reduce the computing sizes of m and q before the sparse coding, which motivates the following joint learning algorithm.

Straightforwardly, with the aim to reduce the time consumption of sparse coding, one popular way is to conduct a down-sampling linear transformation on an input $\mathbf{x}_i$, i.e.,

$$\mathbf{y}_i = \mathbf{V}^\top \mathbf{x}_i$$

with $\mathbf{V} \in \mathbb{R}^{m\times l}, \mathbf{y}_i \in \mathbb{R}^l, l \ll m$. Hence the sparse factorization of $\mathbf{y}_i$ with respect to a common dictionary $\mathbf{D} \in \mathcal{S}(l,k)$ performs as

$$\mathbf{y}_i = \mathbf{D}\boldsymbol{\alpha}_i + \boldsymbol{\epsilon} \tag{11}$$

for all $i = 1, \ldots, n$. Here, the row atoms in $\mathbf{V}$ are orthonormal, i.e., $\mathbf{V}$ is an element of the so-called Stiefel manifold

$$St(m,l) := \{\mathbf{M} \in \mathbb{R}^{m\times l} | \mathbf{M}^\top\mathbf{M} = \mathbf{I}_l\},$$

where $\mathbf{I}_l$ denotes the $l \times l$ identity matrix. Such an orthogonal projection $\mathbf{V} \in St(m,l)$ has been widely used to construct the

efficient dimensionality reduction algorithms, such as standard Principal Component Analysis (PCA) and LDA [7], [23].

By solving the elastic-net problem on $\mathbf{y}$ over $\mathbf{D}$, Eq. (4) performs as

$$\boldsymbol{\alpha}^*_{\mathbf{x}}(\mathbf{V},\mathbf{D}) := \underset{\boldsymbol{\alpha}\in\mathbb{R}^k}{\operatorname{argmin}} \tfrac{1}{2}\|\mathbf{V}^\top\mathbf{x}-\mathbf{D}\boldsymbol{\alpha}\|_2^2+\lambda_1\|\boldsymbol{\alpha}\|_1+\tfrac{\lambda_2}{2}\|\boldsymbol{\alpha}\|_2^2, \tag{12}$$

with $\lambda_1 \in \mathbb{R}^+$ and $\lambda_2 \in \mathbb{R}^+$.

All the possible solutions to the elastic net problem (12) share a convenient fact that, the sparse representation with respect to a specific dictionary is unique. Thus, each sparse vector $\boldsymbol{\alpha}^*_{\mathbf{x}}(\mathbf{V},\mathbf{D})$ can be treated as an implicit function in $\mathbf{x}$, $\mathbf{V}$ and $\mathbf{D}$. Under certain assumptions, there exists a closed form expression for $\boldsymbol{\alpha}^*_{\mathbf{x}}(\mathbf{V},\mathbf{D})$ over variables $\mathbf{x}$, $\mathbf{V}$ and $\mathbf{D}$, which will be discussed in detail in Section IV-A. Furthermore, as addressed in Section IV-A, the sample-wise function $\boldsymbol{\alpha}^*_{\mathbf{x}}(\mathbf{V},\mathbf{D})$ is locally differentiable with respect to $\mathbf{x}$, $\mathbf{V}$ and $\mathbf{D}$, and the first-order derivatives of such a sparse representation have closed-form expressions. With sparse representations of all samples being calculated, specific learning algorithms can be directly applied to these sparse coefficients to extract further representations. The sparse coding associated with its follow-up algorithms could form a joint learning system. Therefore, the local differentiability of $\boldsymbol{\alpha}^*_{\mathbf{x}}(\mathbf{V},\mathbf{D})$ with respect to $\mathbf{x}$, $\mathbf{V}$ and $\mathbf{D}$ could lead to the following framework of adapting learning dictionary to the task of joint three-layer discrimination learning in Section III-B, and deep CNN in Section III-C.

B. Jointly learning discriminative features on sparse representations

As suggested by the work of [20], [21], [25], [42], [43], further processing on the sparse representation is capable of unveiling discriminative underlying information, potentially for supervised learning task. We further assume that the sparse coefficients carry more discriminant information than the original data space. In what follows, we construct a cost function, which allows to jointly learn both the sparsifying dictionary and the two-layer orthogonal transformations in the framework of trace quotient maximization.

We consider a set of data samples $\mathbf{X}_i = [\mathbf{x}_{i1},\ldots,\mathbf{x}_{in_i}] \in \mathbb{R}^{m\times n_i}$ with $i = 1,\ldots,c$, where $c > 1$ indicates the number of classes and n_i refers to the number of data samples in the corresponding i-th class. The projected samples are denoted by $\mathbf{y}_i = [\mathbf{y}_{i1},\ldots,\mathbf{y}_{in_i}] \in \mathbb{R}^{l\times n_i}$. The sparse representations are confined to the solutions of the sparse regression problem in Eq. (4). The corresponding sparse coefficients are denoted by $\boldsymbol{A}_i = [\boldsymbol{\alpha}_{i1},\ldots,\boldsymbol{\alpha}_{in_i}] \in \mathbb{R}^{k\times n_i}$, and $\mathbf{A} = [\boldsymbol{A}_1,\ldots,\boldsymbol{A}_c] \in \mathbb{R}^{k\times n}$.

Straightforwardly, one can construct a linear discriminant analysis problem as

$$\underset{\mathbf{U}\in St(k,d)}{\operatorname{argmax}} \frac{\operatorname{tr}(\mathbf{U}^\top\boldsymbol{\mathcal{B}}\mathbf{U})}{\operatorname{tr}(\mathbf{U}^\top\boldsymbol{\mathcal{W}}\mathbf{U})}, \tag{13}$$

where $\boldsymbol{\mathcal{B}} \in \mathbb{R}^{k\times k}$ is the covariance matrix of the centre of all classes in the sparse feature space, while $\boldsymbol{\mathcal{W}} \in \mathbb{R}^{k\times k}$ is the sum of with-in classes covariance matrices. Therein, $\mathbf{U} \in St(k,d)$ is an orthogonal transformation for learning LD discriminative features. Let $\overline{\boldsymbol{\alpha}}_i \in \mathbb{R}^k$ be the centre of the i-th class. The with-in class covariance matrix is computed by

$$\boldsymbol{\mathcal{W}} = \sum_{i=1}^{c}\sum_{j=1}^{n_i}(\boldsymbol{\alpha}_{ij}-\overline{\boldsymbol{\alpha}}_i)(\boldsymbol{\alpha}_{ij}-\overline{\boldsymbol{\alpha}}_i)^\top = \mathbf{AWA}^\top, \tag{14}$$

with

$$\mathbf{W} := \mathbf{I}_n - \sum_{i=1}^{c}\frac{1}{c}\mathbf{e}_i\mathbf{e}_i^\top,$$

where $\mathbf{e}_i$ is an n-dimensional vector with $\mathbf{e}_i(\iota) = 1$ if $i = c_\iota$; 0 otherwise. Therein, $\mathbf{I}_n$ denotes the $n\times n$ identity matrix, and c_ι denotes the label of ι-th sample, $\iota = 1,2,\cdots,n$.

Let $\overline{\boldsymbol{\alpha}} \in \mathbb{R}^k$ be the centre of all classes. Similarly, we compute the between class covariance matrix by

$$\boldsymbol{\mathcal{B}} = \sum_{i=1}^{c}(\overline{\boldsymbol{\alpha}}_i-\overline{\boldsymbol{\alpha}})(\overline{\boldsymbol{\alpha}}_i-\overline{\boldsymbol{\alpha}})^\top = \mathbf{ABA}^\top, \tag{15}$$

with

$$\mathbf{B} := \sum_{i=1}^{n_i}\frac{1}{n_i}\mathbf{e}_i\mathbf{e}_i^\top - \frac{1}{n}\mathbf{1}_n\mathbf{1}_n^\top.$$

Here, $\mathbf{1}_n = [1,\cdots,1]^\top \in \mathbb{R}^n$.

It is easy to see that solutions of the trace quotient problem in Eq. (13) is invariant with respect to orthonormal basis changes of $\mathbf{U}$, namely,

$$f(\mathbf{U}\boldsymbol{\Theta}) = f(\mathbf{U})$$

for any orthogonal matrix $\boldsymbol{\Theta} \in \mathbb{R}^{d\times d}$. Hence, it induces a function on the Grassmann manifold $Gr(d,k)$. In this work, we identify $Gr(d,k)$ as the set of all rank-d symmetric projection operators on $\mathbb{R}^k$ [44], i.e.,

$$Gr(d,k) := \{\mathbf{P}\in\mathbb{R}^{k\times k} | \mathbf{P}=\mathbf{P}^\top, \mathbf{P}^2=\mathbf{P}, \operatorname{tr}\mathbf{P}=d\}.$$

Thus, one can straightforwardly represent the trace quotient function of Eq. (13) as a first-order smooth optimization problem on a Grassmann manifold

$$\widetilde{f}\colon Gr(d,m)\to\mathbb{R}, \qquad \widetilde{f}(\mathbf{P}) := \frac{\operatorname{tr}(\mathbf{ABA}^\top\mathbf{P})}{\operatorname{tr}(\mathbf{AWA}^\top\mathbf{P})}, \tag{16}$$

where $\mathbf{P} = \mathbf{UU}^\top$.

It is worth noticing that when $\mathbf{P}$ is given, $\mathbf{U}$ is obtained by the QR-decomposition

$$\mathbf{P} = \mathbf{UR}, \tag{17}$$

where $\mathbf{U} \in St(k,d)$ is orthogonal and $\mathbf{R}$ is invertible upper triangular with nonnegative entries on the diagonal, cf. [44], [45].

Now, let us denote by $\mathbf{A}_{\mathbf{X}}(\mathbf{V},\mathbf{D}) \in \mathbb{R}^{k\times n}$ the sparse representation of $\mathbf{y}$ with respect to $\mathbf{V}$ and $\mathbf{D}$. By employing all ingredients, we propose to construct the cost function in sparse representations as

$$\begin{aligned} &f\colon St(m,l)\times\mathcal{S}(l,k)\times Gr(d,k)\to\mathbb{R},\\ &f(\mathbf{V},\mathbf{D},\mathbf{P}) := \frac{\operatorname{tr}\left(\mathbf{A}_{\mathbf{X}}(\mathbf{V},\mathbf{D})\mathbf{B}\mathbf{A}_{\mathbf{X}}^\top(\mathbf{V},\mathbf{D})\mathbf{P}\right)}{\operatorname{tr}\left(\mathbf{A}_{\mathbf{X}}(\mathbf{V},\mathbf{D})\mathbf{W}\mathbf{A}_{\mathbf{X}}^\top(\mathbf{V},\mathbf{D})\mathbf{P}+\sigma\mathbf{I}_k\right)}\\ &\qquad = \frac{\operatorname{tr}\left(\boldsymbol{\mathcal{B}}\mathbf{P}\right)}{\operatorname{tr}\left(\boldsymbol{\mathcal{W}}\mathbf{P}+\sigma\mathbf{I}_k\right)}, \end{aligned} \tag{18}$$

where

$$\boldsymbol{\mathcal{B}} = \mathbf{A}_{\mathbf{X}}(\mathbf{V},\mathbf{D})\mathbf{B}\mathbf{A}_{\mathbf{X}}^{\top}(\mathbf{V},\mathbf{D})$$

and

$$\boldsymbol{\mathcal{W}} = \mathbf{A}_{\mathbf{X}}(\mathbf{V},\mathbf{D})\mathbf{W}\mathbf{A}_{\mathbf{X}}^{\top}(\mathbf{V},\mathbf{D}).$$

f is a smooth function defined on the product manifold of the Stiefel manifold, the Oblique manifold and the Grassmann manifold. In Eq. (18), $\sigma > 0$ is used to guarantee $\boldsymbol{\mathcal{W}}\mathbf{P} + \sigma\mathbf{I}_k$ to be nonsingular, i.e., $\mathrm{tr}(\boldsymbol{\mathcal{W}}\mathbf{P} + \sigma\mathbf{I}_k) > 0$ always hold. In this work, we refer to Eq. (18) as the *JoopLow* function.

C. Optimizing JoopLow in convolutional representation space

Let $\mathbf{Z} := [\mathbf{Z}_1, \ldots, \mathbf{Z}_c] \in \mathbb{R}^{m\times n}$ be a collection of c classes, each of which contains n_c raw imagery samples, $n = cn_c$. The preliminary training features that are extracted by deep convolutional neural networks (CNN) [27], [28] are obtained via a CNN mapping

$$g\colon \mathbf{z}_i \mapsto \mathbf{x}_i, \qquad \text{for all } i = 1, \ldots, n, \tag{19}$$

hence, as discussed in Section III-B, $\mathbf{x}_i$ is taken to feed the *JoopLow* system. According to the pipeline depicted in Fig. 2, the whole learning system, namely, *CNN-JoopLow*, involves CNN parameters, and a triple of matrix parameters, i.e., $\mathbf{V}, \mathbf{D}, \mathbf{P}$. The *JoopLow* paradigm is employed as full connections in the original CNN framework. Hereafter, we will represent the complete *CNN-JoopLow* scheme by its parameters

$$\boldsymbol{\theta}_{\textit{CNN-JoopLow}} = \{\boldsymbol{\theta}_{\mathrm{CNN}}, \mathbf{V}, \mathbf{D}, \mathbf{P}\},$$

where $\boldsymbol{\theta}_{\mathrm{CNN}}$ denotes all CNN parameters.

Finally, by regarding Eq. (18) as the global main cost function and using the chain rule, based on which backpropagation (BP) could be used to train the whole network. In order to make such a deep network perform well, an appropriate initialization of the parameters is necessary. We randomly select a certain number of samples from the training data, then the CNN parameters are initialized by performing pretraining in a greedy layer-wise fashion using its original network. Once given the CNN features, we initialize the parameters $\mathbf{V}, \mathbf{D}, \mathbf{P}$ by using the strategy of Section IV-C. We empirically show in Section VI that the proposed deep coding approach yields improved performance in large scale image datasets.

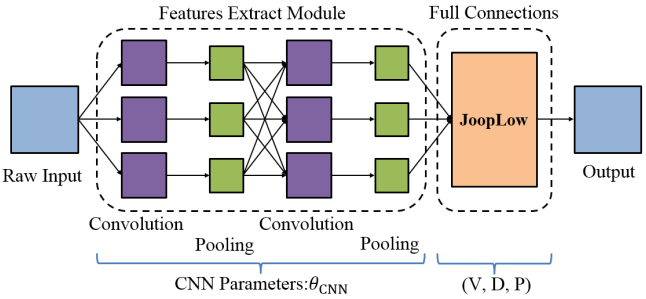

Fig. 2. The classic structure of CNN, it consists of two modules: Feature extraction module (FEM) and Full connection module (FC). This figure depicts the architecture of *CNN-JoopLow*, in which the convolutional layers have the same structures as the corresponding classical CNN models, whereas all FC layers are replaced with the *JoopLow* layer.

IV. Optimization Algorithm for *JoopLow*

Since the optimization on CNN architectures is nowadays well established, we present the optimization algorithm in *JoopLow*. Recalling the feasible set of solutions to maximize the cost function in Eq. (18) is restricted to the product manifold of the Stiefel manifold, the Oblique manifold and the Grassmann manifold. In what follows, we adopt the gradient descent (GD) algorithm on smooth manifolds, to maximize the cost function f on $St(m,l) \times \mathcal{S}(l,k) \times Gr(d,k)$. In the rest of this paper, $\mathbf{A}_{\mathbf{X}}(\mathbf{V},\mathbf{D})$ is shortly denoted by $\mathbf{A}$ in some places.

A. Local Differentiability and Euclidean Gradients

The key requirement for developing a gradient algorithm to minimize the cost function f is the differentiability of sparse representation with respect to its parameters $\mathbf{x}$, $\mathbf{V}$, $\mathbf{D}$ and $\mathbf{P}$, which is implicitly included in the term f. In this subsection, we investigate the (local) differentiability of the sparse representation in the dictionary from the perspective of global analysis. Then we derive the gradients of f with respect to $\mathbf{V}$, $\mathbf{D}$ and $\mathbf{P}$.

Let us first discuss the sparse solution to the elastic net problem (12). Given the set of indices of the non-zero entries of the solution $\boldsymbol{\alpha}^* = [\varphi_1^*, \ldots, \varphi_k^*]^{\top} \in \mathbb{R}^k$, which is defined as $\Lambda := \{i \in \{1, \ldots, k\} | \varphi_i^* \neq 0\}$, then the solution $\boldsymbol{\alpha}^*$ has a closed-form expression as

$$\boldsymbol{\alpha}_{\mathbf{x}}^*(\mathbf{V},\mathbf{D}) := \left(\mathbf{D}_{\Lambda}{}^{\top}\mathbf{D}_{\Lambda} + \lambda_2 I_l\right)^{-1}\left(\mathbf{D}_{\Lambda}{}^{\top}\mathbf{V}^{\top}\mathbf{x} - \lambda_1 \mathbf{s}_{\Lambda}\right), \tag{20}$$

where $\mathbf{s}_{\Lambda} \in \{\pm 1\}^{|\Lambda|}$ carries the signs of $\boldsymbol{\alpha}_{\mathbf{x}_{\Lambda}}^*$, $\mathbf{D}_{\Lambda} \in \mathbb{R}^{l\times|\Lambda|}$ is the subset of $\mathbf{D}$ in which the index of atoms (rows) fall into support Λ. Furthermore, with a reasonable assumption that the dictionary $\mathbf{D}$ is suitably incoherent, the solution $\boldsymbol{\alpha}_{\mathbf{x}}^*(\mathbf{V},\mathbf{D})$ as given in Eq. (20) is a locally twice differentiable function at $\mathbf{D}$.

Let us denote $\mathbf{K} := \mathbf{D}_{\Lambda}^{\top}\mathbf{D}_{\Lambda} + \lambda_2\mathbf{I}_l$. The first-order derivatives of $\boldsymbol{\alpha}_{\mathbf{x}}^*(\mathbf{V},\mathbf{D})$ with respect to $\mathbf{D}$ and $\mathbf{V}$, in the directions $\mathbf{H} \in T_{\mathbf{D}}\mathcal{S}(l,k)$, $\boldsymbol{\Xi} \in \mathbf{T}_{\mathbf{V}}\mathbf{St}(\mathbf{m},\mathbf{l})$ are respectively computed by

$$\begin{aligned}\mathcal{D}\,\boldsymbol{\alpha}_{\mathbf{x}}^*(\mathbf{V},\mathbf{D})\mathbf{H} = &\mathbf{K}^{-1}\mathbf{H}_{\Lambda}^{\top}\mathbf{V}^{\top}\mathbf{x} - \mathbf{K}^{-1}(\mathbf{D}_{\Lambda}^{\top}\mathbf{H}_{\Lambda} \\ &+\mathbf{H}_{\Lambda}^{\top}\mathbf{D}_{\Lambda})\cdot\mathbf{K}^{-1}\left(\mathbf{D}_{\Lambda}^{\top}\mathbf{V}^{\top}\mathbf{x} - \lambda_1\mathbf{s}_{\Lambda}\right),\end{aligned} \tag{21}$$

and

$$\mathcal{D}\,\boldsymbol{\alpha}_{\mathbf{x}}^*(\mathbf{V},\mathbf{D})\boldsymbol{\Xi} = \mathbf{K}^{-1}\mathbf{D}_{\Lambda}^{\top}\boldsymbol{\Xi}_{\Lambda}^{\top}\mathbf{x}. \tag{22}$$

Therein, $T_{\mathbf{D}}\mathcal{S}(l,k)$ and $T_{\mathbf{V}}St(m,l)$ denote the tangent space of $\mathcal{S}(l,k)$ at $\mathbf{D}$, and the tangent space of $St(m,l)$ at $\mathbf{V}$, respectively. The technical concepts of them will be shown in Section IV. Similarly, the first-order derivatives of $\boldsymbol{\alpha}_{\mathbf{x}}^*(\mathbf{V},\mathbf{D})$ with respect to $\mathbf{x}$ in the direction $\mathbf{h}$ is

$$\mathcal{D}\,\boldsymbol{\alpha}_{\mathbf{x}}^*(\mathbf{V},\mathbf{D})\mathbf{h} = \mathbf{K}^{-1}\mathbf{D}_{\Lambda}^{\top}\mathbf{D}_{\Lambda}^{\top}\mathbf{h}. \tag{23}$$

With the first-order derivatives of $\boldsymbol{\alpha}_{\mathbf{x}}^*(\mathbf{V},\mathbf{D})$ at hand, in order to conveniently construct the gradient method for maximizing the function f, computing the Euclidean gradients of f with respect to the arguments $\mathbf{V}$, $\mathbf{D}$, and $\mathbf{P}$ is necessary.

The following gives ingredients of Euclidean gradient of f. Firstly, it is easy to compute the Euclidean gradient of f with respect to $\mathbf{P}$ by

$$\nabla f(\mathbf{P}) = \frac{\mathrm{tr}(\boldsymbol{\mathcal{W}}\mathbf{P}+\sigma\mathbf{I})\boldsymbol{\mathcal{B}}^\top - \mathrm{tr}(\boldsymbol{\mathcal{B}}\mathbf{P})\boldsymbol{\mathcal{W}}^\top}{\mathrm{tr}^2(\boldsymbol{\mathcal{W}}\mathbf{P}+\sigma\mathbf{I})} \tag{24}$$

where $\boldsymbol{\mathcal{W}} = \mathbf{AWA}^\top, \boldsymbol{\mathcal{B}} = \mathbf{ABA}^\top$.

Using some shorthand notation, let us denote $\mathbf{r} := [\mathbf{r}_1, \ldots, \mathbf{r}_n] = \mathbf{PAB} \in \mathbb{R}^{k\times n}$ and $\boldsymbol{\nu} := [\boldsymbol{\nu}_1, \ldots, \boldsymbol{\nu}_n] = \mathbf{PAW} + \sigma\mathbf{I} \in \mathbb{R}^{k\times n}$. Based on the solution in Eq. (21), the gradient of f in Eq. (18) with respect to $\mathbf{D}$ can be given by

$$\begin{aligned}\nabla f(\mathbf{D}) = 2\sum_{i=1}^{n}\mathcal{R}\{&\frac{\mathbf{V}^\top\mathbf{x}_i\mathbf{r}_{i,\Lambda_i}^\top\mathbf{K}_i^{-1} - \mathbf{D}_{\Lambda_i}\mathbf{K}_i^{-1}\widehat{\boldsymbol{\rho}}_i\mathbf{K}_i^{-1}}{\mathrm{tr}(\mathbf{AWA}^\top\mathbf{P}+\sigma\mathbf{I})}\\ &- \frac{\left(\mathbf{V}^\top\mathbf{x}_i\boldsymbol{\nu}_{i,\Lambda_i}^\top\mathbf{K}_i^{-1} - \mathbf{D}_{\Lambda_i}\mathbf{K}_i^{-1}\widehat{\omega}_i\mathbf{K}_i^{-1}\right)\mathrm{tr}(\mathbf{A}^\top\mathbf{r})}{\mathrm{tr}^2(\mathbf{AWA}^\top\mathbf{P}+\sigma\mathbf{I})}\}\end{aligned} \tag{25}$$

with

$$\begin{aligned}\boldsymbol{\rho}_i &:= (\mathbf{D}_{\Lambda_i}^\top\mathbf{V}^\top\mathbf{x}_i - \lambda_1\mathbf{s}_{\Lambda_i})\mathbf{r}_{i,\Lambda_i}^\top,\ \widehat{\boldsymbol{\rho}}_i := \boldsymbol{\rho}_i + \boldsymbol{\rho}_i^\top,\\ \boldsymbol{\omega}_i &:= (\mathbf{D}_{\boldsymbol{\omega}_i}^\top\mathbf{V}^\top\mathbf{x}_i - \lambda_1\mathbf{s}_{\Lambda_i})\boldsymbol{\nu}_{i,\Lambda_i}^\top,\ \widehat{\omega_i} := \boldsymbol{\omega}_i + \boldsymbol{\omega}_i^\top,\end{aligned} \tag{26}$$

where $\mathcal{R}(\mathbf{Z}_\Lambda)$ denotes the full vector $\mathbf{Z}$ of $\mathbf{Z}_\Lambda$. We then compute the Euclidean gradient of f with respect to $\mathbf{V}$ by

$$\begin{aligned}\nabla f(\mathbf{V}) =& 2\sum_{i=1}^{n}\mathcal{R}\{\frac{\mathbf{x}_i\mathbf{K}_i^{-1}\mathbf{D}_{\Lambda_i}\mathbf{r}_{i,\Lambda_i}^\top}{\mathrm{tr}(\mathbf{AWA}^\top\mathbf{P}+\sigma\mathbf{I})}\\ &- \frac{\left(\mathbf{x}_i\mathbf{K}_i^{-1}\mathbf{D}_{\Lambda_i}\boldsymbol{\nu}_{i,\Lambda_i}^\top\right)\mathrm{tr}(\mathbf{A}^\top\mathbf{r})}{\mathrm{tr}^2(\mathbf{AWA}^\top\mathbf{P}+\sigma\mathbf{I})}\}.\end{aligned} \tag{27}$$

The computation of above Euclidean gradients of f with respect to $\mathbf{V}$, $\mathbf{D}$, and $\mathbf{P}$ gives the way to determine their following Riemannian gradients of f.

B. A gradient descent algorithm on the Product of Matrix Manifolds

Let $\boldsymbol{\mathcal{M}} := St(m,l)\times\mathcal{S}(l,k)\times Gr(d,k)$ be a product manifold of a Riemannian submanifold of $\mathbb{R}^{m\times l}\times\mathbb{R}^{l\times k}\times\mathbb{R}^{k\times k}$, and let $f\colon \boldsymbol{\mathcal{M}} \to \mathbb{R}$ be the differentiable cost function of Eq.(18). The general solution to the optimization problem in Eq. (18) on the matrix manifold, an element of $\boldsymbol{\mathcal{M}}$, is denoted by $\boldsymbol{\Theta} \in \boldsymbol{\mathcal{M}}, \boldsymbol{\Theta} := (\mathbf{V}, \mathbf{D}, \mathbf{P})$. Some required concepts on $\boldsymbol{\mathcal{M}}$ are depicted in Fig. 3 to alleviate the understanding. For a detailed overview on optimization on matrix manifolds, we refer the interested reader to [18], [37]. Before introducing the GD algorithm on $\boldsymbol{\mathcal{M}}$, we first compute the Riemannian gradients of f with respect to $\mathbf{V}$, $\mathbf{D}$ and $\mathbf{P}$.

As depicted in Fig. 3, the Riemannian gradient of f is a tangent vector that points in the direction of steepest ascent of f on $\boldsymbol{\mathcal{M}}$. By the product structure of $St(m,l)\times\mathcal{S}(l,k)\times Gr(d,k)$, the tangent space of $\boldsymbol{\mathcal{M}}$ at a point $\boldsymbol{\Theta} := (\mathbf{V}, \mathbf{D}, \mathbf{P}) \in \boldsymbol{\mathcal{M}}$ is simply the product of all individual tangent spaces, i.e.,

$$T_{\boldsymbol{\Theta}}\boldsymbol{\mathcal{M}} := T_{\mathbf{V}}St(m,l)\times T_{\mathbf{D}}\mathcal{S}(l,k)\times T_{\mathbf{P}}Gr(d,k). \tag{28}$$

Each tangent space of $\boldsymbol{\mathcal{M}}$ is endowed with the Riemannian metric inherited from the surrounding Euclidean space, which for two points $\boldsymbol{\mathcal{Q}} = (\mathbf{Q}_1, \mathbf{Q}_2, \mathbf{Q}_3) \in T_{\boldsymbol{\Theta}}\boldsymbol{\mathcal{M}}$ and $\mathbf{E} = (\mathbf{E}_1, \mathbf{E}_2, \mathbf{E}_3) \in T_{\boldsymbol{\Theta}}\boldsymbol{\mathcal{M}}$ is given by

$$\langle\boldsymbol{\mathcal{Q}}, \mathbf{E}\rangle := \mathrm{tr}(\mathbf{Q}_1^\top\mathbf{E}_1) + \mathrm{tr}(\mathbf{Q}_2^\top\mathbf{E}_2) + \mathrm{tr}(\mathbf{Q}_3^\top\mathbf{E}_3). \tag{29}$$

Then, by computing the first derivation of f at $(\mathbf{V}, \mathbf{D}, \mathbf{P})$ in tangent direction $(\mathbf{H}_\mathbf{V}, \mathbf{H}_\mathbf{D}, \mathbf{H}_\mathbf{P}) \in T_{\boldsymbol{\Theta}}\boldsymbol{\mathcal{M}}$, we can get the Riemannian gradient of f at $(\mathbf{V}, \mathbf{D}, \mathbf{P})$ as

$$\mathcal{G}(\boldsymbol{\Theta}) = \left(\boldsymbol{\tau}_\mathbf{V}(\nabla f(\mathbf{V})), \boldsymbol{\Pi}_\mathbf{D}(\nabla f(\mathbf{D})), \boldsymbol{\pi}_\mathbf{P}(\nabla f(\mathbf{P}))\right), \tag{30}$$

where $\left(\boldsymbol{\tau}_\mathbf{V}(\mathbf{Z}_1), \boldsymbol{\Pi}_\mathbf{D}(\mathbf{Z}_2), \boldsymbol{\pi}_\mathbf{P}(\mathbf{Z}_3)\right)$ is the orthogonal projection of some arbitrary points $(\mathbf{Z}_1, \mathbf{Z}_2, \mathbf{Z}_3) \in \mathbb{R}^{m\times l}\times\mathbb{R}^{l\times k}\times\mathbb{R}^{k\times k}$ onto the tangent space $T_{\boldsymbol{\Theta}}\boldsymbol{\mathcal{M}}$ with respect to the inner product of Eq. (29).

Let us denote by $\nabla f(\mathbf{V})$, $\nabla f(\mathbf{D})$, $\nabla f(\mathbf{P})$ the Euclidean gradients of f with respect to $\mathbf{V}$, $\mathbf{D}$, $\mathbf{P}$, which have been computed via Eq. (25), Eq. (24) and Eq. (27), respectively. Then, the Riemannian gradient of f with respect to the arguments $\mathbf{V}$, $\mathbf{D}$, and $\mathbf{P}$ are given by

$$\mathcal{G}_\mathbf{V}(\boldsymbol{\Theta}) = \nabla f(\mathbf{V}) - \mathbf{V}(\nabla f(\mathbf{V}))^\top\mathbf{V}, \tag{31}$$

$$\mathcal{G}_\mathbf{D}(\boldsymbol{\Theta}) = \nabla f(\mathbf{D}) - \mathbf{D}\,\mathrm{diag}(\mathbf{D}^\top\nabla f(\mathbf{D})), \tag{32}$$

and

$$\mathcal{G}_\mathbf{P}(\boldsymbol{\Theta}) = [\mathbf{P}, [\mathbf{P}, \nabla f(\mathbf{P})]], \tag{33}$$

with the matrix commutator $[\mathbf{E}, \mathbf{Q}] := \mathbf{EQ} - \mathbf{QE}$. Therein, $\mathrm{ddiag}(\mathbf{Z})$ is the diagonal matrix whose entries on the diagonal are those of $\mathbf{Z}$. The above formulas regarding the geometry of $St(m,l)\times\mathcal{S}(l,k)\times Gr(d,k)$ are derived in [37].

Finally, by assembling the Riemannian gradients on the underlying manifolds, some smooth solvers, like stochastic gradient descent (SGD) algorithm or conjugate gradient (CG) algorithm on $St(m,l)\times\mathcal{S}(l,k)\times Gr(d,k)$, are straightforward. In this section, we employ a classical heuristic in SGD algorithms [20], i.e., using a minibatch strategy in each iteration instead of a single one, to train our proposed *JoopLow*. We briefly summarize a SGD algorithm for maximizing the function f as defined in Eq. (18), cf. Algorithm 1.

In Algorithm 1, the key is how to update the point $\boldsymbol{\Theta}^{(j)}$ to the point $\boldsymbol{\Theta}^{(j+1)}$ along the commonly used *geodesic*, denoted by the red curve $\Gamma_{\boldsymbol{\Theta}^{(j)}}(\gamma\mathbf{H})$ in Fig. 3, which are often more computationally demanding, cf. [37]. In this work, we adopt an alternative approach, based on the concept of retraction, introduced as follows.

A retraction $\mathfrak{R}_{\boldsymbol{\Theta}}\colon T_{\boldsymbol{\Theta}}\mathcal{M} \to \mathcal{M}$ is a smooth mapping from the tangent space $T_{\boldsymbol{\Theta}}\mathcal{M}$ to the manifold, such that the evaluation $\mathfrak{R}_{\boldsymbol{\Theta}}(0) = \boldsymbol{\Theta}$ and the derivative $\mathcal{D}\Gamma_{\boldsymbol{\Theta}}(0)\colon T_{\boldsymbol{\Theta}}\mathcal{M} \to T_{\boldsymbol{\Theta}}\mathcal{M}$ is the identity mapping. Formally, let us define $\mathbf{H}_\mathbf{V}, \mathbf{H}_\mathbf{D}, \mathbf{H}_\mathbf{P}$ the search directions at $\mathbf{V}, \mathbf{D}, \mathbf{P}$, the retractions defined on $St(m,l), \mathcal{S}(l,k), Gr(d,k)$ are

$$\begin{cases}\mathfrak{R}_\mathbf{V}(\gamma\mathbf{H}_\mathbf{V}) &:= \left(\mathbf{V}+\gamma\mathbf{H}_\mathbf{V}\right)_Q,\\ \mathfrak{R}_\mathbf{D}(\gamma\mathbf{h}_\mathbf{D}) &:= [\mathfrak{R}_{\mathbf{d}_1}(\gamma\mathbf{h}_{\mathbf{d}_1}), \cdots, \mathfrak{R}_{\mathbf{d}_k}(\gamma\mathbf{h}_{\mathbf{d}_k})],\\ \mathfrak{R}_\mathbf{P}(\gamma\mathbf{H}_\mathbf{P}) &:= \zeta_\mathbf{P}(\gamma\mathbf{H}_\mathbf{P})\mathbf{P}\zeta_\mathbf{P}(\gamma\mathbf{H}_\mathbf{P})^\top\end{cases} \tag{34}$$

with

$$\mathfrak{R}_\mathbf{d}(\gamma\mathbf{h}_\mathbf{d}) = \frac{\mathbf{d}+\gamma\mathbf{h}_\mathbf{d}}{\|\mathbf{d}+\gamma\mathbf{h}_\mathbf{d}\|_2},$$

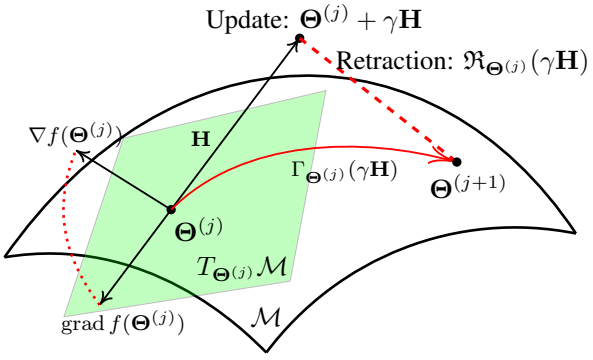

Fig. 3. Some concepts of the Geometric SGD algorithm can be visualized in this figure. At first, it shows two nearby points $\mathbf{\Theta}^{(j)}$ and $\mathbf{\Theta}^{(j+1)}$ on a manifold $\mathcal{M}$ together with the tangent space at $\mathbf{\Theta}^{(j)}$ (green area). Tangent space : $T_{\mathbf{\Theta}^{(j)}}\mathcal{M}$, a real vector space containing all possible directions that tangentially pass through $\mathbf{\Theta}^{(j)}$; Secondly, it shows a update from the point $\mathbf{\Theta}^{(j)}$ to the point $\mathbf{\Theta}^{(j+1)}$ in a search direction $\mathbf{H}\in T_{\mathbf{\Theta}^{(j)}}\mathcal{M}$ along the curve $\Gamma_{\mathbf{\Theta}^{(j)}}(\gamma\mathbf{H})$. The geodesic $\Gamma_{\mathbf{\Theta}^{(j)}}(\gamma\mathbf{H})$in the direction of $\mathbf{H}$ connects the two points $\mathbf{\Theta}^{(j)}$ and $\mathbf{\Theta}^{(j+1)}$, with γ being the step size. Thirdly, it describes that how to approximate the geodesic $\Gamma_{\mathbf{\Theta}^{(j)}}(\gamma\mathbf{H})$ by using the retraction $\mathfrak{R}_{\mathbf{\Theta}^{(j)}}(\gamma\mathbf{H})$. Finally, it introduces the gradient at $\mathbf{\Theta}^{(j)}$, i.e., the Euclidean gradient $\nabla f(\mathbf{\Theta}^{(j)})$ and its projection onto the tangent space at $\mathbf{\Theta}^{(j)}$, called Riemannian gradient: $\mathrm{grad}\, f(\mathbf{\Theta}^{(j)})\in T_{\mathbf{\Theta}^{(j)}}\mathcal{M}$.

Algorithm 1: A *SGD-JoopLow* Algorithm.

Input : Given training set $\mathbf{X}\in\mathbb{R}^{m\times n}$, which is divided into η batches and each batch with the size of τ, i.e., $\mathbf{X}:=[\mathbf{X}_1,\ldots,\mathbf{X}_n]\in\mathbb{R}^{m\times\eta\tau}$, parameters λ_1, λ_2, σ and λ ;

Output: $(\mathbf{V}^*,\mathbf{D}^*,\mathbf{P}^*)\in St(m,l)\times\mathcal{S}(l,k)\times Gr(d,k)$;

Step 1: Generate initialization for $(\mathbf{V}^{(0)},\mathbf{D}^{(0)},\mathbf{P}^{(0)})$, and set $j=-1$;

Step 2: Set $j=j+1$;

Step 3: Update sparse codes $\mathbf{A}_{g(\mathbf{X}_j)}(\mathbf{V}^{(j)},\mathbf{D}^{(j)},\mathbf{P}^{(j)})$ for each $\boldsymbol{\alpha}_{\mathbf{x}_i}(\mathbf{V}^{(j)},\mathbf{D}^{(j)})$ using Elastic Net in Eq. (4) ;

Step 4: Update $\mathbf{H}^{(j+1)}\leftarrow-\mathrm{grad}\, f(\mathbf{V}^{(j)},\mathbf{D}^{(j)},\mathbf{P}^{(j)})$;

Step 5: Update $(\mathbf{V}^{(j+1)},\mathbf{D}^{(j+1)},\mathbf{P}^{(j+1)})\leftarrow(\mathbf{V}^{(j)},\mathbf{D}^{(j)},\mathbf{P}^{(j)})+\gamma\mathbf{H}^{(j)}$, where γ is computed by employing a backtracking line search, cf. [18] ;

Step 6: Project $\mathbf{V}^{(j+1)},\mathbf{D}^{(j+1)},\mathbf{P}^{(j+1)}$ onto $St(m,l)\times\mathcal{S}(l,k)\times Gr(d,k)$ by computing Retractions defined in Eq. (34) ;

Step 7: If $\left\|\mathbf{H}^{(j+1)}\right\|$ is small enough, stop. Otherwise, go to Step 2;

$$\zeta_{\mathbf{P}}(\gamma\mathbf{H}_{\mathbf{P}}):=\left(\mathbf{I}_k+\gamma(\mathbf{H}_{\mathbf{P}}\mathbf{P}-\mathbf{P}\mathbf{H}_{\mathbf{P}})\right)_Q.$$

Therein, $(\cdot)_Q$ is the unique QR decomposition of an invertible matrix, i.e., all diagonal entries of the upper triangular part are positive. An intuitive description for retractions is illustrated in Fig. 3.

Once the Riemannian gradients are obtained, the way we used for updating the point is via **Step 4** to **Step 6** in Algorithm 1. Furthermore, by treating the CNN feature as a differentiable input function, the parameters $\boldsymbol{\theta}_{\textit{CNN-JoopLow}}$ of *CNN-JoopLow* could be easily solved by using Algorithm 1.

C. Initialization

Let us denote $(\mathbf{V}_0,\mathbf{D}_0,\mathbf{P}_0)$ by the initialization of parameters $(\mathbf{V},\mathbf{D},\mathbf{P})$. At first, $\mathbf{V}$ is initialized by the projection matrix of PCA. We then use K-SVD [4] to learn a sub-dictionary in the reduced space for each class, and then combine all the sub-dictionaries as a shared dictionary $\mathbf{D}_0$. Generally speaking, given initialized $\mathbf{D}_0$, $\mathbf{U}$ could be initialized via applying classical LDA [7] on sparse representations with respect to $\mathbf{D}_0$, denoted by $\mathbf{U}_0^\top$, then $\mathbf{P}_0=\mathbf{U}_0\mathbf{U}_0^\top$. Note that, we shortly call the LDA in the sparse domain with respect to $\mathbf{D}_0$ as *SparJoopLow*, which is the initialization of *JoopLow*. However, when the dataset is huge, directly applying LDA is often difficult. In this case, we randomly select a certain number of samples from the training data, and then employ the classical LDA on SR to get the orthogonal projection $\mathbf{U}_0^\top$.

V. Numerical Experiments

In this section, we investigate the performance of the proposed *JoopLow* for discrimination learning of multi-class large-scale imagery objects. For the convenience of descriptions, we refer to the proposed *JoopLow* associated with the preliminary representation learners, e.g. SPP and CNN, as the shorthands, *SPP-JoopLow* and *CNN-JoopLow*, respectively. Additionally, as described in Section IV-C, we refer to their sequential learning counterpart, which directly applies a LDA on the corresponding sparse representations, as *SPP-SparJoopLow* and *CNN-SparJoopLow*, respectively. Before showing our experiments, we briefly discuss the issues of choosing the experimental parameters.

A. Experimental Settings

Throughout all experiments, we consistently set $\sigma=10^{-3}$ in Eq. (18). Let n be the number of all signals which contain c classes, we use n_{train}, n_{test} to denote the number of total training samples and the number of total testing samples, respectively. Usually, we set $n=n_{\text{train}}+n_{\text{test}}$. For parameters λ_1,λ_2 in Eq.(4), in order to put an emphasis on sparse solutions, we choose $\lambda_2\in(0,\frac{\lambda_1}{10})$, as described in [46].

Building upon multi-class large-scale objects categorization, besides the CNN that is described in Section III-C, another popular way is to first detect various local image features, such as HOG and SIFT, and then quantize them into discrete "visual words" over a codebook or dictionary. Finally, it computes a fixed-length SPP vector of acquired "visual words", cf. [29]–[31]. We shortly call it *SIFT/HOG-SPP* representation. The related codes are publicly online available. In this work, the SIFT/HOG descriptor is extracted from $s\times s$ pixel patches densely sampled from each image. $s=16$ for SIFT and $s=16,25,31$ for HOG. The dimension of each SIFT/HOG descriptor is 128. A codebook with the size of 1024 is learned for coding SIFT/HOG features, cf. [30]. We then divide the image into 4×4, 3×3 and 1×1 subregions, i.e., 21 bins. The final SPP representations are computed with the size $m=21504$, and hence fed into the proposed *JoopLow*. In what follows, we refer to it as the *SPP-JoopLow*, in comparison to *CNN-JoopLow*.

By following the architecture of proposed *CNN-JoopLow* (see Fig. 2 and Section III-C), it assembles between the state-of-the-art CNN methods and the basic *JoopLow*. Generally speaking, the advantages of *CNN-JoopLow* are independent to the convolutional network architectures. We investigate four different network architectures in existing publications, i.e., ConvNet-5 [47], OverFeat-7 [39], AlexNet-5 [38], ZF-5 [40] and VGG-16 [27]. We then show *JoopLow* improves the accuracy of all these architectures on the multi-class large-scale objects categorization problem. In these networks, the convolutional layers have the same structures as the corresponding baseline models, whereas all Full Connection (FC) layers after the final pooling layer are replaced with the *JoopLow* layer.

Another architecture used in this work is called *SPP-net* [28], which combines the convolutional networks and the aforementioned SPP architecture, i.e., it first computes several layers convolutional features, and then follow up a SPP layer to generate a fixed-length representation. As shown in [28], we adopt the OverFeat-7 [39] for images with the fixed cropped size 224×224. The pyramid is $\{6 \times 6, 3 \times 3, 2 \times 2, 1 \times 1\}$, i.e., 50 bins. Finally, the extracted SPP feature vectors are fed into the FC layers, or the *JoopLow* in this work. The related codes for *SIFT/HOG-SPP* and *SPP-net* are both publicly online available.

During the training process, the input images to CNN based methods are resized so that the smaller dimension is 256, cropping the center 256×256 region, and then, a 224×224 crop is picked from the center or the four corners from the entire image. The only preprocessing we do is subtracting the mean RGB value, computed on the training set, from each pixel. Usually, we follow the settings reported in the respective reference papers [27], [28].

The main goal of this work is to learn appropriate LD representations of images. In what follows, we denote m, l, k, d, by the dimension of SPP/CNN representation space, the dictionary atom, the orthogonal projected space, and the targeted LD discriminative feature space, respectively. As suggested in [7], the targeted low dimensionality d is set to be $d = c - 1$. In this experiment, we investigate the impact of the choice of dimension parameters for l, k to the performance of *SIFT-SPP-JoopLow* by applying on Caltech-101 dataset [48]. As depicted in Fig. 4, *SIFT-SPP-JoopLow* model is examined in terms of recognition accuracy with respect to different dimension parameters of l, k. It is clear that, when $l \geq 512$ and $k \geq 2040$, the tested *CNN-JoopLow* method performs well for this specific task.

Finally, in the experiments, we employ a classical heuristic in SGD algorithms [27], i.e., using a minibatch strategy in each iteration instead of a single one, to train our proposed *JoopLow*. In practice, the batch size $\tau = 8c$ for datasets except ImageNet has given good results in our experiments. For ImageNet dataset [38], SGD with a mini-batch size of 256 is used to update the parameters. The learning rate starts from 0.01 in conjunction with a momentum term of 0.9.

In the following, in order to verify the effectiveness of the proposed *JoopLow*, we perform the categorization experiments on objects or scenes that have different scales, complex backgrounds and multiple classes, such as the images from ImageNet dataset [35], Caltech-101 dataset [48], and Caltech-256 dataset [35].

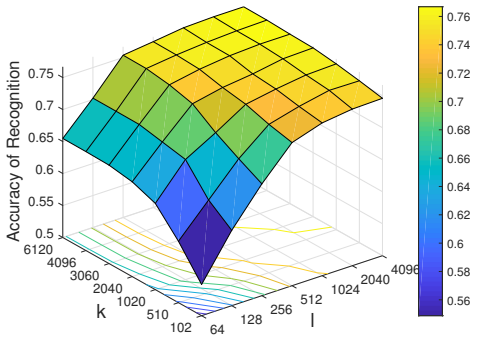

Fig. 4. Impact of the parameters l, k to the recognition rate on the Caltech-101 dataset with $n_{\text{train}} = 30$.

TABLE II
COMPARISON OF RESULTS ON ILSVRC−2012 DATASET.

Methods	Top-1 val.	Top-5 val.	Top-1 test
DeCAF-5 [49]	–	–	19.2%
ZF-5 [40]	37.5%	16.0%	16.1%
ZF-5 JoopLow	36.6%	15.4%	16.0%
AlexNet-5 [38]	38.1%	16.4%	16.4%
AlexNet-5 JoopLow	37.0%	16.2%	16.1%
VGG-16 [27]	24.7%	7.5%	7.3%
VGG-16 JoopLow	22.6%	6.7%	7.0%
OverFeat-7 [39]	35.7%	14.2%	–
OverFeat-7 JoopLow	33.0%	12.8%	–
SPP-net+OverFeat-7 [28]	27.86%	9.14%	9.08%
SPP-net+OverFeat-7 JoopLow	26.33%	9.08%	9.3%
ResNet-152 [50]	21.43%	5.71%	–
X-Ception+ResNet [51]	21.0%	5.5%	–
Inception V4+ResNet [52]	21.0%	5.0%	–

B. Object Categorization on ImageNet 2012

In this subsection, we present the image classification results achieved by the described *CNN-JoopLow* architectures on a subset of ImageNet dataset [53], used in ILSVRC 2012 − 2014 competition, namely, ILSVRC−2012 dataset in the work. The dataset includes roughly 1000 images in each of 1000 categories with an average size of around 400×350, and is split into three sets: 1.28 million training images set, 50K validation images set, and 100K testing images set with held-out class labels. Our training algorithm follows the practices of the previous work [27], [38], [40].

Our implementation is based on the publicly available code of cuda convnet [38] and Tensorflow[1]. All the models are trained for 50 epochs on 4 Titan GPUs. The classification performances are evaluated using the *Top-1, Top-5 Error Rates* in the Validation Set of ImageNet 2012 and the *top-1 test set error rate* in the Testing Set of ImageNet 2012, abbreviated as "Top-1 val.", "Top-5 val.", and "Top-1 test", respectively [38].

By following the proposed *CNN-JoopLow* (see Fig. 2), which assembles between the state-of-the-art CNN methods and the basic *JoopLow*, our results on ILSVRC−2012 are summarized in Table II. In Table II, the numbers in DeCAF-5

[1] https://www.tensorflow.org/

[49], ResNet-152 [50], ZF-5 [40], AlexNet-5 [40], OverFeat-7 [39] and SPP-net+OverFeat-7 [28] indicate the number of convolutional layers. For example, ZF-5 [40] denotes the architecture of ZF (Zeiler and Ferguss (ZF)) model with five convolutional layers. In order to reduce the training time, we now explore the ability of feature extraction layers of classic CNNs to generalize to their *JoopLow* counterparts. For example, we utilize the model parameters of ZF-5 [40] to be the initialization of *ZF-5-JoopLow*. This strategy has been heuristically proved to be very efficient by our numerical experiments.

As can be seen from Table II, our deep *CNN-JoopLow* could improve the performance of their conventional CNN counterparts. We achieve error rate reduction within $1.1\% \sim 2.1\%$ of their reported values on the ImageNet 2012 validation set. These results are lower than that produced by the very deeper approaches of ResNet [50] and its recently derivative methods, such as X-Ception [51] and Inception V4 [52], which could also be easily combined with the *CNN-JoopLow* architecture. However, they requires larger computing resources and prohibitive training efforts, due to the larger number of layers (e.g. 152 layers for ResNet).

For multi-class large-scale objects categorization, one important aspect is surely the number of labelled samples. We compare the *CNN-JoopLow* counterparts of two state of the art CNN based algorithms, i.e., *VGG-16-JoopLow* versus *VGG-16* [27], *ZF-5-JoopLow* versus *ZF-5* [40]. For these CNN methods, we use the same settings of CNN layers as reported in their original references. Our results in Fig. 5 show that three *CNN-JoopLow* methods consistently outperform all their CNN counterparts. It is worth noticing that with an decreasing number of labeled samples, *CNN-JoopLoow* methods demonstrate greater advantages over their conventional counterparts.

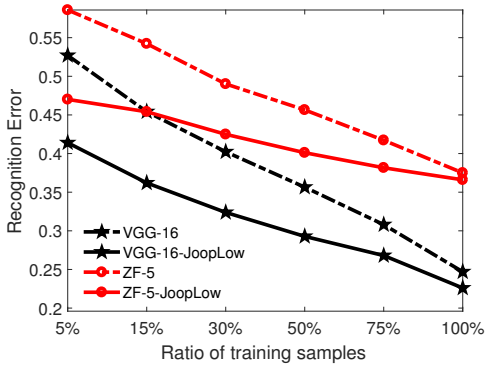

Fig. 5. Impact of the number of labelled samples to the recognition rate on the ILSVRC−2012 dataset. The curves denote Top-1 Error Rates in the Validation Set of ImageNet 2012.

C. Object Categorization on Caltech dataset

The experiments above show the importance of the *JoopLow* part of the proposed ImageNet model in obtaining state-of-the-art CNN performance. In the following, we investigate its effectiveness for classifying object categories in small scale datasets, e.g. Caltech-101 dataset [48] and Caltech-256 dataset [35].

The Caltech-101 dataset contains 9144 images from 102 classes (101 object categories and a background class) with 31 to about 800 images per category., The images being in medium resolution, i.e., about 300×300 pixels. Learning on Caltech-101 dataset is often considered to be hard, since the number of images per category varies significantly from 31 to 800. The Caltech-256 dataset holds more samples, i.e., $30,607$ images falling into 256 categories with resolution from 113×150 to 960×1280. Each category has a minimum of 80 images. Unlike the Caltech-101 dataset, this dataset contains multiple objects in various poses at different locations within the images. Existence of background clutter and occlusion result in higher intraclass diversity, which makes the categorization task even harder.

On both Caltech-101&256 datasets, we follow the common experimental setups in [28]–[30], and then generate several random splits into training and test data, finally report the average recognition performance across the splits. As common, on Caltech-101, we randomly sample 5, 15 and 30 images per category for training and the rest images for testing. On Caltech-256, we also randomly generated 3 splits, each of which contains 15, 30 or 60 training images per class, and the rest is used for testing.

Considering in short of the training samples, we now explore the ability of ImageNet trained feature extraction layers, i.e., the convolutional layers, to generalize to other datasets, namely Caltech-101 and Caltech-256. This is well-known transferring capability of convolutional layers that has been verified by various classical CNNs, cf. [27], [40], [49]. For example, for the *ZF-5 JoopLow*, we keep layers $1-8$ (i.e., convolutional layers and *JoopLow* layers) of our ImageNet-pretrained model fixed, further to be the initialization of *ZF-5 JoopLow* on Caltech dataset. Hence, we fine-tune the whole system and train a new classifier as follow-up strategy (for the appropriate number of classes) by using the training images of the new dataset. We refer to this learning paradigm as the *ImageNet-pretrained JoopLow* in the following, or abbreviated as "pretrained" CNN model in Table III.

It is worth mentioning that there is an intersection between ImageNet training dataset and Caltech dataset, which may trick the final results. By following the [40], we identified these few "overlap" images and removed them from our Imagenet training set and then retrained our Imagenet models.

We set $\lambda_1 = 5 \times 10^{-2}, \lambda_2 = 10^{-5}$, and $d = 101$. For the case of $n_{\text{train}} = 15$ in Caltech-101, we set $l = 1530$, $k = 2040$, the average sparsity is 5.5627 for each reduced SPP feature vector, 7.3762 for each reduced CNN feature vector. For the case of $n_{\text{train}} = 30$ in Caltech-101, we set $l = 2040$, $k = 3060$, the average sparsity is 7.5890 and 8.9011, respectively. In this work, once the final LD representations are obtained, $k-$NN (k Nearest Neighbors) is employed as a classifier. For Caltech-256, we set $l = 1280$, $d = 255$. For the cases of $n_{\text{train}} = 30, 60$, we set $k = 2048, 2560$, respectively. Finally, we use Gaussian SVM for classifying the LD features of Caltech-256 data. Table III shows the mean recognition rates for both the Caltech datasets averaged for 3 runs, in comparison with some conventional methods and state-of-the-art CNN approaches. As can be seen from the Table III, five conclusions are summarized as follows.

At first, it is clear that *SIFT/HOG-SPP-JoopLow* and

TABLE III
CLASSIFICATION PERFORMANCE ON CALTECH-101 & CALTECH-256 DATASETS FOR THE PROPOSED *JoopLow* FRAMEWORK, WITH COMPARISONS TO APPROACHES FROM THE LITERATURE. SPP-NET IS SPECIFIED BY SPP-NET BASED ON OVERFEAT-7. "NO PRETRAINED" METHOD INDICATES THE CNN MODEL WITHOUT BEING PRETRAINED ON IMAGENET DATASET, AND VICE VERSA.

Methods		(a) Caltech-101; Accuracy (%)			(b) Caltech-256 ; Accuracy (%)		
		$n_{train} = 5$	$n_{train} = 15$	$n_{train} = 30$	$n_{train} = 15$	$n_{train} = 30$	$n_{train} = 60$
Hand-crafted methods	KSPM [31]	–	56.4	64.4 ± 0.8	–	23.34 ± 0.42	29.51 ± 0.52
	ScSPM+SVM [29]	–	67.0 ± 0.4	73.2 ± 0.5	27.73	34.02 ± 0.35	40.14 ± 0.91
	LLC+SVM [30]	51.15	65.43	73.44	34.36	41.19	47.68
	LSc [54]	–	66.10	–	29.99	35.74 ± 0.10	40.32 ± 0.32
	SRC [19], [55]	48.8	$47.4 \sim 48.3$	$57.8 \sim 58.5$	27.86	33.33	–
	SSPIC [55]	55.1	$65.5 \sim 66.5$	$71.5 \sim 72.5$	–	–	–
	LC-KSVD [23]	54.0	67.7	73.6	28.9	34.32	–
	M-HMP [56]	–	–	81.4 ± 0.33	40.5 ± 0.4	48.0 ± 0.2	55.2 ± 0.3
	SIFT/HOG-SPP - JoopLow	56.44	$74.8 \sim 74.9$	$77.3 \sim 77.5$	35.2	$39.4 \sim 39.5$	$48.9 \sim 50.0$
	SIFT/HOG-SPP-PCA-JoopLow	55.60	$73.6 \sim 73.8$	$76.4 \sim 76.5$	34.4	$37.1 \sim 37.3$	$46.1 \sim 46.3$
CNN based methods	No pretrained ZF-5 [40]	15.9 ± 3.2	22.8 ± 1.5	46.5 ± 1.7	9.0 ± 1.4	22.5 ± 0.7	38.8 ± 1.4
	No pretrained *ZF-5-JoopLow*	20.1 ± 2.0	39.2 ± 0.6	56.3 ± 0.5	19.6 ± 0.7	37.2 ± 0.6	49.3 ± 0.7
	Pretrained ZF-5 [40]	79.5 ± 0.6	83.8 ± 0.5	86.5 ± 0.5	65.7 ± 0.2	70.6 ± 0.2	74.2 ± 0.3
	Pretrained *ZF-5-JoopLow*	82.0 ± 0.4	85.7 ± 0.3	87.4 ± 0.3	68.3 ± 0.3	72.2 ± 0.2	76.0 ± 0.2
	No pretrained VGG-16 [27]	–	28.0 ± 1.3	52.1 ± 0.9	–	24.9 ± 1.0	42.1 ± 0.9
	No pretrained *VGG-16-JoopLow*	–	42.2 ± 0.7	57.8 ± 0.9	–	31.4 ± 0.8	51.4 ± 0.9
	Pretrained VGG-16 [27]	–	87.2 ± 0.2	91.8 ± 0.1	–	78.3 ± 0.2	85.0 ± 0.2
	Pretrained *VGG-16 PCA JoopLow*		85.2 ± 0.2	89.3 ± 0.2		75.7 ± 0.2	83.9 ± 0.3
	Pretrained *VGG-16-JoopLow*	–	89.1 ± 0.3	92.4 ± 0.2	–	80.2 ± 0.3	86.6 ± 0.3
	No pretrained SPP-net [28]	–	–	48.2 ± 0.8	–	–	–
	No pretrained *SPP-net JoopLow*	–	–	57.9 ± 0.7	–	–	–
	Pretrained SPP-net [28]	–	–	93.4 ± 0.5	–	–	–
	Pretrained *SPP-net JoopLow*	–	–	93.5 ± 0.3	–	–	–

SIFT/HOG-SPP-PCA-JoopLow methods outperform by far the conventional shallow learning approaches consistently, such as one-layer sparse coding methods, i.e., ScSPM+SVM, LLC+SVM, SRC, SSPIC, and LC-KSVD, but they are easily defeated by a recent multi-layer sparse coding method, M-HMP [56] in Table III. M-HMP learns features through multiple layers of sparse coding, associated with multiple paths, to capture multiple aspects of discriminative structures. Furthermore, from Table III, it also indicates that the deep CNN based methods has an overwhelming advantage over traditional hand-crafted methods. This is due to the power of convolutional layers on feature extraction, in case of the availability of much larger training sets. Such a progress in deep learning shows the importance of learning features through multiple layers.

Secondly, the ImageNet-pretrained CNN approaches bring at least 14% improvement over conventional single layer approaches in terms of categorization accuracy. The main reason is that CNN can explore deeper essential class information that are hidden in raw imagery data. Furthermore, the ability of ImageNet-pretrained feature extraction layers has been transferred to the model applied on Caltech-101 dataset. All these show the power of the ImageNet pretrained CNN feature extractor, i.e., the transferring capability of deep CNNs.

Thirdly, it can be found in Table III that the proposed *CNN-JoopLow* methods could significantly improve the recognition accuracy in comparison with their conventional CNN counterparts, especially when the number of training samples decreases. This suggests that *CNN-JoopLow* has the advantage on training small-sample datasets.

Fourthly, as for comparison, we also perform the *JoopLow* on PCA-projected CNN/SPP features. Table III shows that the recognition result of *SIFT-SPP* + PCA + *JoopLow* is slightly behind the record of *SIFT-SPP* + *JoopLow*. But for *CNN-JoopLow*, *VGG-16-JoopLow* has much better records than *VGG-16-PCA-JoopLow*. It is clear from this result that, the joint optimization system of *JoopLow* could highly improve the performance.

Finally, for *CNN* based approaches, we also try a second strategy of training a model from scratch. For example, we reset $1 - 8$ layers of *ZF-5 JoopLow* to random values and train them, as well as the classifier, on the training images of the Caltech datasets. They are denoted by "No pretrained" method in Table III. However, CNN based approaches training large models from scratch, i.e., without ImageNet-pretrained initialization, may heavily suffer from the overfitting, and the results decrease drastically. For the Caltech-101 dataset with $n_{\text{train}} = 15$, "No pretrained" methods like the *ZF-5* and the *ZF-5 JoopLow* only achieve 22.8% and 39.2%, against the 83.8% and 85.7% for the "Pretrained" *ZF-5* and the "Pretrained" *ZF-5 JoopLow*. The similar results are also shown by VGG-16 series and SPP-net series in Table III. It is apparent from all these comparisons that training a large convnet on such a small dataset is impossible. On the other hand, *CNN-JoopLow* methods without ImageNet pretraining stage are shown to have more advantages than their CNN counterparts. These results benefit from the trace quotient cost based on double orthogonal projections and sparse representation.

Fig. 6(a) plots the confusion matrix using hand-crafted *SIFT-SPP* + *JoopLow*. It shows that 13 categories in Caltech101 achieve the 100% classification accuracy, i.e., *accordion, snoopy, inline_skate, car_side, dollar_bill, garfield, metronome, okapi, pagoda, scissors, minaret, trilobite* and *stop_sign*. On the other hand, the categories with highest confusion are *water lilly* (Acc. $= 28.57\%$) and *lotus* (Acc. $= 58.33\%$), i.e., 42.86% of *water lilly* are identified as *lotus*

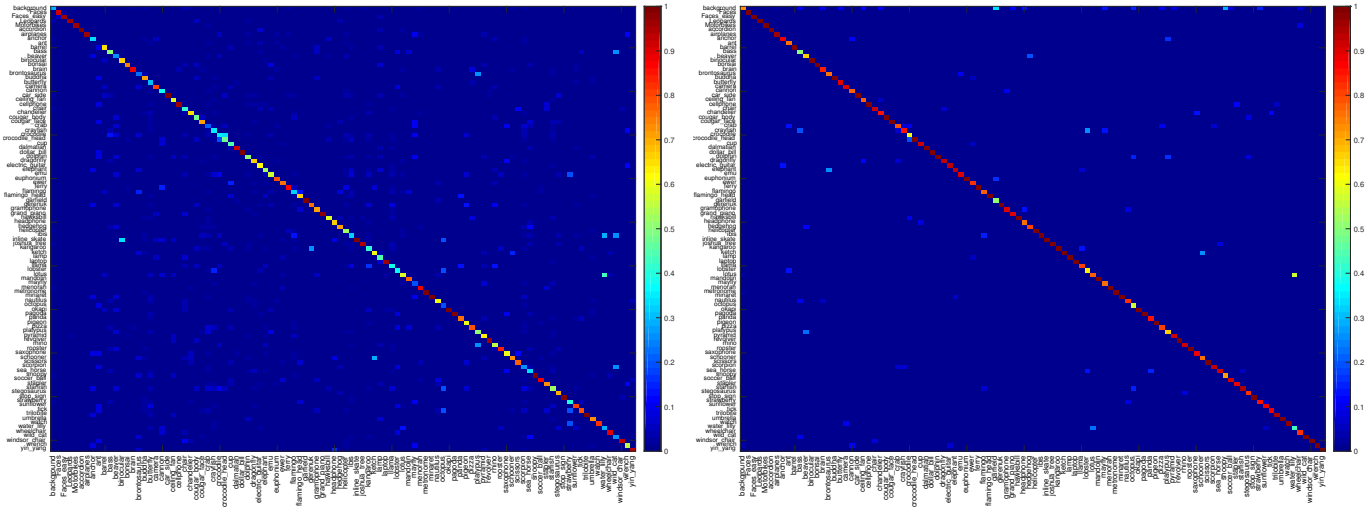

(a) Confusion matrix of *SIFT-SPP + JoopLow*

(b) Confusion matrix of *VGG-16-JoopLow*

Fig. 6. Confusion matrix for Caltech-101 with 30 training images per class, and the rest 6084 images for testing, shown using the jet color scale from Matlab. Dark red indicates 100% while dark blue indicates 0%, with a gradient from warm to cool colors in between (see scale, right). A perfect matrix would be dark blue matrix except for a dark red diagonal.

and 13.89% of *lotus* are identified as *water lilly*. Fig. 6(b) plots the confusion matrix using *VGG-16-JoopLow* with $n_{train} = 30$. Compared to *SIFT-SPP + JoopLow*, 44 categories achieve the 100% classification accuracy. The categories with highest confusion are also *water lilly* (Acc. $= 42.86\%$) and *lotus* (Acc. $= 76.92\%$), i.e., 57.14% of *water lilly* are identified as *lotus* and 23.08% of *lotus* are identified as *water lilly*. These comparisons show the promising improvement of CNN based *JoopLow* against the hand-crafted *SIFT-SPP* based *JoopLow*.

VI. Conclusions

This paper proposed a joint discriminant learning approach, called *JoopLow*, in order to find LD discriminative representations of multi-class large-scale imagery objects. The parameters of *JoopLow* cost function are well defined on the product manifold of the Stiefel manifold, the Oblique manifold and the Grassmann manifold. By using the differentiability of solutions of sparse regression, *JoopLow* could be well adapted to the state-of-the-art CNN methods, and ensembles a differentiable deep learning architecture, namely *CNN-JoopLow*. Hence, the *CNN-JoopLow* could be efficiently solved by a proposed Riemannian stochastic gradient descent algorithm. The *CNN-JoopLow* takes the advantages of CNN, sparse dictionary learning and orthogonal projections. The experimental results show stronger competitive performance in comparison with the state-of-the-arts. In future, we consider to extend *JoopLow* to deeper CNN architectures, applying in more general case, such as general dimensionality reduction and unsupervised clustering problem with orthogonality constraints.

References

[1] Yoshua Bengio, Aaron Courville, and Pascal Vincent, "Representation learning: A review and new perspectives," *IEEE Transactions on Pattern Analysis and Machine Intelligence*, vol. 35, no. 8, pp. 1798–1828, 2013.

[2] John P Cunningham and Zoubin Ghahramani, "Linear dimensionality reduction: Survey, insights, and generalizations," *Journal of Machine Learning Research*, vol. 16, pp. 2859–2900, 2015.

[3] Yann LeCun, Yoshua Bengio, and Geoffrey Hinton, "Deep learning," *Nature*, vol. 521, no. 7553, pp. 436–444, 2015.

[4] Michal Aharon, Michael Elad, and Alfred Bruckstein, "K-SVD: An algorithm for designing overcomplete dictionaries for sparse representation," *IEEE Transactions on Signal Processing*, vol. 54, no. 11, pp. 4311–4322, 2006.

[5] Yoshua Bengio and Aaron Courville, *Deep learning of representations*, pp. 1–28, Springer Berlin Heidelberg, Berlin, Heidelberg, 2013.

[6] Sam T Roweis and Lawrence K Saul, "Nonlinear dimensionality reduction by locally linear embedding," *Science*, vol. 290, no. 5500, pp. 2323–2326, 2000.

[7] Peter N Belhumeur, João P Hespanha, and David Kriegman, "Eigenfaces vs. fisherfaces: Recognition using class specific linear projection," *IEEE Transactions on Pattern Analysis and Machine Intelligence*, vol. 19, no. 7, pp. 711–720, 1997.

[8] Andrew Y. Ng, Michael I. Jordan, and Yair Weiss, "On spectral clustering: Analysis and an algorithm," in *Advances in Neural Information Processing Systems*. 2002, pp. 849–856, MIT Press.

[9] Joshua B Tenenbaum, Vin De Silva, and John C Langford, "A global geometric framework for nonlinear dimensionality reduction," *Science*, vol. 290, no. 5500, pp. 2319–2323, 2000.

[10] Rémi Gribonval, Rodolphe Jenatton, Francis Bach, Martin Kleinsteuber, and Matthias Seibert, "Sample complexity of dictionary learning and other matrix factorizations," *IEEE Transactions on Information Theory*, vol. 61, no. 6, pp. 3469–3486, 2015.

[11] Deng Cai, Xiaofei He, and Jiawei Han, "Semi-supervised discriminant analysis," in *IEEE 11th International Conference on Computer Vision (ICCV)*. IEEE, 2007, pp. 1–7.

[12] F. R. Bach K. Fukumizu and M. I. Jordan., "Dimensionality reduction for supervised learning with reproducing kernel hilbert spaces," *Journal of Machine Learning Research*, vol. 5, pp. 73–99, 2004.

[13] Mukund N Desai and Rami S Mangoubi, "Robust subspace learning and detection in laplacian noise and interference," *IEEE transactions on signal processing*, vol. 55, no. 7, pp. 3585–3595, 2007.

[14] Xian Wei, Li Yuanxiang, Hao Shen, Xiang Weidong, and Yi Lu Murphey, "Joint learning sparsifying linear transformation for low-resolution image synthesis and recognition," *Pattern Recognition*, vol. 66, no. 7, pp. 412–424, 2017.

[15] Xian Wei, *Learning Image and Video Representations Based on Sparsity Priors*, Shaker Verlag GmbH, Aachen, Germany, 2017.

[16] D. L. Donoho, "Compressed sensing," *IEEE Transactions on Information Theory*, vol. 52, no. 4, pp. 1289–1306, 2006.

[17] Xian Wei, Hao Shen, Yuanxiang Li, Xuan Tang, Fengxiang Wang, Martin Kleinsteuber, and Yi Lu Murphey, "Reconstructible nonlinear dimensionality reduction via joint dictionary learning.," *IEEE transactions on neural networks and learning systems*, vol. 30, no. 1, pp. 175–189, 2019.

[18] Simon Hawe, Matthias Seibert, and Martin Kleinsteuber, "Separable dictionary learning," in *Proceedings of the IEEE Conference on Computer Vision and Pattern Recognition (CVPR)*. IEEE, June 2013, pp. 438–445.

[19] John Wright, Allen Y Yang, Arvind Ganesh, S Shankar Sastry, and Yi Ma, "Robust face recognition via sparse representation," *IEEE transactions on pattern analysis and machine intelligence*, vol. 31, no. 2, pp. 210–227, 2009.

[20] Julien Mairal, Francis Bach, and Jean Ponce, "Task-driven dictionary learning," *IEEE Transactions on Pattern Analysis and Machine Intelligence*, vol. 34, no. 4, pp. 791–804, 2012.

[21] Xian Wei, Hao Shen, and Martin Kleinsteuber, "Trace quotient meets sparsity: A method for learning low dimensional image representations," in *Proceedings of the IEEE Conference on Computer Vision and Pattern Recognition (CVPR)*, 2016, pp. 5268–5277.

[22] Meng Yang, Lei Zhang, Xiangchu Feng, and David Zhang, "Sparse representation based fisher discrimination dictionary learning for image classification," *International Journal of Computer Vision*, vol. 109, no. 3, pp. 209–232, 2014.

[23] Zhuolin Jiang, Zhe Lin, and Larry S Davis, "Label consistent K-SVD: learning a discriminative dictionary for recognition," *IEEE Transactions on Pattern Analysis and Machine Intelligence*, vol. 35, no. 11, pp. 2651–2664, 2013.

[24] Xian Wei, Yuanxiang Li, Hao Shen, Fang Chen, Martin Kleinsteuber, and Zhongfeng Wang, "Dynamical textures modeling via joint video dictionary learning," *IEEE Transactions on Image Processing*, vol. 26, no. 6, 2017.

[25] Jianchao Yang, Kai Yu, and Thomas Huang, "Supervised translation-invariant sparse coding," in *Proceedings of the IEEE Conference on Computer Vision and Pattern Recognition (CVPR)*. IEEE, 2010, pp. 3517–3524.

[26] Julien Mairal, Jean Ponce, Guillermo Sapiro, Andrew Zisserman, and Francis R Bach, "Supervised dictionary learning," in *Advances in neural information processing systems*, 2009, pp. 1033–1040.

[27] Karen Simonyan and Andrew Zisserman, "Very deep convolutional networks for large-scale image recognition," *arXiv preprint arXiv:1409.1556*, 2014.

[28] Kaiming He, Xiangyu Zhang, Shaoqing Ren, and Jian Sun, "Spatial pyramid pooling in deep convolutional networks for visual recognition," *IEEE Transactions on Pattern Analysis and Machine Intelligence*, vol. 37, no. 9, pp. 1904–1916, 2015.

[29] Jianchao Yang, Kai Yu, Yihong Gong, and Thomas Huang, "Linear spatial pyramid matching using sparse coding for image classification," in *Proceedings of the IEEE Conference on Computer Vision and Pattern Recognition (CVPR)*. IEEE, 2009, pp. 1794–1801.

[30] Jinjun Wang, Jianchao Yang, Kai Yu, Fengjun Lv, Thomas Huang, and Yihong Gong, "Locality-constrained linear coding for image classification," in *Proceedings of the IEEE Conference on Computer Vision and Pattern Recognition (CVPR)*. IEEE, 2010, pp. 3360–3367.

[31] Svetlana Lazebnik, Cordelia Schmid, and Jean Ponce, "Beyond bags of features: Spatial pyramid matching for recognizing natural scene categories," in *Proceedings of the IEEE Conference on Computer Vision and Pattern Recognition (CVPR)*. IEEE, 2006, vol. 2, pp. 2169–2178.

[32] Florian Schroff, Dmitry Kalenichenko, and James Philbin, "Facenet: A unified embedding for face recognition and clustering," in *Proceedings of the IEEE conference on computer vision and pattern recognition*, 2015, pp. 815–823.

[33] François Chollet, "Xception: Deep learning with depthwise separable convolutions," in *IEEE Conference on Computer Vision and Pattern Recognition (CVPR)*. IEEE, 2017, pp. 1800–1807.

[34] Christian Szegedy, Sergey Ioffe, Vincent Vanhoucke, and Alexander A Alemi, "Inception-v4, inception-resnet and the impact of residual connections on learning," in *AAAI*, 2017, vol. 4, p. 12.

[35] Gregory Griffin, Alex Holub, and Pietro Perona, "Caltech-256 object category dataset," 2007.

[36] H. Zou and T. Hastie, "Regularization and variable selection via the elastic net," *Journal of the Royal Statistical Society, Series B*, vol. 67, no. 2, pp. 301–320, 2005.

[37] P-A Absil, Robert Mahony, and Rodolphe Sepulchre, *Optimization algorithms on matrix manifolds*, Princeton University Press, 2008.

[38] Alex Krizhevsky, Ilya Sutskever, and Geoffrey E Hinton, "Imagenet classification with deep convolutional neural networks," in *Advances in neural information processing systems*, 2012, pp. 1097–1105.

[39] Pierre Sermanet, David Eigen, Xiang Zhang, Michaël Mathieu, Rob Fergus, and Yann LeCun, "Overfeat: Integrated recognition, localization and detection using convolutional networks," in *International Conference on Learning Representations (ICLR)*, 2014.

[40] Matthew D Zeiler and Rob Fergus, "Visualizing and understanding convolutional networks," in *European conference on computer vision (ECCV)*. Springer, 2014, pp. 818–833.

[41] Li-Fen Chen, Hong-Yuan Mark Liao, Ming-Tat Ko, Ja-Chen Lin, and Gwo-Jong Yu, "A new lda-based face recognition system which can solve the small sample size problem," *Pattern recognition*, vol. 33, no. 10, pp. 1713–1726, 2000.

[42] Junbin Gao, Qinfeng Shi, and Tibério S Caetano, "Dimensionality reduction via compressive sensing," *Pattern Recognition Letters*, vol. 33, no. 9, pp. 1163–1170, 2012.

[43] Ehsan Elhamifar and Rene Vidal, "Sparse subspace clustering: Algorithm, theory, and applications," *IEEE Transactions on Pattern Analysis and Machine Intelligence*, vol. 35, no. 11, pp. 2765–2781, 2013.

[44] U. Helmke and J. B. Moore, *Optimization and Dynamical Systems*, Springer, Berlin, 1994.

[45] Martin Kleinsteuber and Knut Huper, "An intrinsic CG algorithm for computing dominant subspaces," in *Proceedings of the Thirty-Second IEEE International Conference on Acoustics, Speech, and Signal Processing (ICASSP)*. IEEE, 2007, vol. 4, pp. 1402–1405.

[46] Hui Zou and Trevor Hastie, "Regularization and variable selection via the elastic net," *Journal of the Royal Statistical Society: Series B (Statistical Methodology)*, vol. 67, no. 2, pp. 301–320, 2005.

[47] Yann LeCun, Léon Bottou, Yoshua Bengio, and Patrick Haffner, "Gradient-based learning applied to document recognition," *Proceedings of the IEEE*, vol. 86, no. 11, pp. 2278–2324, 1998.

[48] Li Fei-Fei, Rob Fergus, and Pietro Perona, "Learning generative visual models from few training examples: An incremental bayesian approach tested on 101 object categories," *Computer Vision and Image Understanding*, vol. 106, no. 1, pp. 59–70, 2007.

[49] Jeff Donahue, Yangqing Jia, Oriol Vinyals, Judy Hoffman, Ning Zhang, Eric Tzeng, and Trevor Darrell, "Decaf: A deep convolutional activation feature for generic visual recognition," in *International conference on machine learning*, 2014, pp. 647–655.

[50] Kaiming He, Xiangyu Zhang, Shaoqing Ren, and Jian Sun, "Deep residual learning for image recognition," in *Proceedings of the IEEE conference on computer vision and pattern recognition*, 2016, pp. 770–778.

[51] François Chollet, "Xception: Deep learning with depthwise separable convolutions," *arXiv preprint*, pp. 1610–02357, 2017.

[52] Christian Szegedy, Sergey Ioffe, Vincent Vanhoucke, and Alexander A Alemi, "Inception-v4, inception-resnet and the impact of residual connections on learning.," in *Proceedings of the Thirty-First AAAI Conference on Artificial Intelligence (AAAI)*, 2017, vol. 4, p. 12.

[53] Olga Russakovsky, Jia Deng, Hao Su, Jonathan Krause, Sanjeev Satheesh, Sean Ma, Zhiheng Huang, Andrej Karpathy, Aditya Khosla, Michael Bernstein, Alexander C. Berg, and Li Fei-Fei, "Imagenet large scale visual recognition challenge," *International Journal of Computer Vision (IJCV)*, vol. 115, no. 3, pp. 211–252, 2015.

[54] Shenghua Gao, Ivor Wai-Hung Tsang, and Liang-Tien Chia, "Laplacian sparse coding, hypergraph laplacian sparse coding, and applications," *IEEE Transactions on Pattern Analysis and Machine Intelligence*, vol. 35, no. 1, pp. 92–104, 2013.

[55] Umamahesh Srinivas, Yuanming Suo, Minh Dao, Vishal Monga, and Trac D Tran, "Structured sparse priors for image classification," *IEEE Transactions on Image Processing*, vol. 24, no. 6, pp. 1763–1776, 2015.

[56] Liefeng Bo, Xiaofeng Ren, and Dieter Fox, "Multipath sparse coding using hierarchical matching pursuit," in *Proceedings of the IEEE Conference on Computer Vision and Pattern Recognition*, 2013, pp. 660–667.